

Modeling the timing of Patagonian Ice Sheet retreat in the Chilean Lake District from 22-10 ka

Joshua Cuzzone¹, Matias Romero², Shaun A. Marcott²

¹Joint Institute for Regional Earth System Science and Engineering, University of California, Los Angeles

²Department of Geoscience, University of Wisconsin, Madison

Correspondence to: Joshua K. Cuzzone (Joshua.K.Cuzzone@jpl.nasa.gov)

Abstract

Studying the retreat of the Patagonian Ice Sheet (PIS) during the last deglaciation represents an important opportunity to understand how ice sheets outside the polar regions have responded to deglacial changes in temperature and large-scale atmospheric circulation. At the northernmost extension of the PIS during the last glacial maximum (LGM), the Chilean Lake District (CLD) was influenced by the southern westerly winds (SWW), which strongly modulated the hydrologic and heat budget of the region. Despite progress in constraining the nature and timing of deglacial ice retreat across this area, considerable uncertainty in the glacial history still exists due to a lack of geologic constraints on past ice margin change. Where the glacial chronology is lacking, ice sheet models can provide important insight into our understanding of the characteristics and drivers of deglacial ice retreat. Here we apply the Ice Sheet and Sea-level System Model (ISSM) to simulate the LGM and last deglacial ice history of the PIS across the CLD at high spatial resolution (450 meters). We present a transient simulation of ice margin change across the last deglaciation using climate inputs from the CCSM3 Trace-21ka experiment. At the LGM, the simulated ice extent across the CLD agrees well with the most comprehensive reconstruction of PIS ice history (PATICE). Coincident with deglacial warming, ice retreat ensues after 19ka, with largescale ice retreat occurring across the CLD between 18 and 16.5 ka. By 17 ka the northern portion of the CLD becomes ice free, and by 15 ka, ice only persists at high elevations as mountain glaciers and small ice caps. Our simulated ice history agrees well with PATICE for early deglacial ice retreat but diverges at and after 15 ka, where geologic reconstruction suggest persistence of an ice cap across the southern CLD until 10 ka. However, given the high uncertainty in the geologic reconstruction of the PIS across the CLD during the later deglaciation, this work emphasizes a need for improved geologic constraints on past ice margin change. While deglacial warming drove the ice retreat across this region, sensitivity tests reveal that modest variations in wintertime precipitation (~10%) can modulate the pacing of ice retreat by up to 2 ka, which has implications when comparing simulated outputs of ice margin change to geologic reconstructions. While we find that TraCE-21ka simulates large-scale changes in the SWW across the CLD that are consistent with regional paleoclimate reconstructions, the magnitude of the simulated precipitation changes is smaller than what is found in proxy records. From our sensitivity analysis we can deduce that larger anomalies in precipitation as found in paleoclimate proxies may have had a large impact on modulating deglacial ice retreat, highlighting an additional need to better constrain the deglacial change in the strength, position, and extent of the SWW as it relates to understanding of drivers of deglacial PIS behavior.

Deleted: 3

Deleted: an ensemble of LGM ice sheet model experiments using climate inputs from the Paleoclimate Modelling Intercomparison Project (PMIP4) and

Deleted: We find that although the simulated LGM temperature is primarily responsible for differences in simulated ice geometries, wintertime precipitation also plays an important role in modulating LGM ice sheet volume and extent. The

Formatted: Font color: Text 1

Formatted: Font color: Text 1

Formatted: Font color: Text 1

Formatted: Font color: Text 1

Deleted: simulated deglaciation is found to match existing geologic constraints that indicate widespread ice margin retreat between 18 to 16.5 ka. Following this interval our simulations suggest that the ice sheet retreated rapidly, and by 15 ka onward, only mountain glaciers remained across the CLD in contrast with sparse geologic data that indicate a local ice cap remaining until 10ka. Additionally, our results suggest that modest variations in winter precipitation (~10%) can modulate the pacing of ice retreat by 1-2 ka, which has implications when comparing simulated outputs of ice margin change to geologic reconstructions. Therefore, these LGM and deglacial experiments signify the importance in constraining the deglacial strength, latitudinal position, and extent of the SWW and its influence on the hydrologic and heat budget and also highlight the importance in constraining paleoclimate parameters critical to modelling and understanding the drivers of deglacial PIS behavior. ¶

1 Introduction

During the Last glacial maximum (LGM), the Patagonian Ice Sheet (PIS) covered the Andes mountains from 38°S to 55°S, with an estimated sea-level equivalent ice volume of 1.5 meters (Davies et al., 2020). At the northernmost extent of the PIS, across an area presently known as the Chilean Lake District (CLD), the LGM to deglacial ice behavior and related climate forcings has been a subject of historical interest (Mercer, 1972; Porter, 1981; Lowell et al., 1995; Andersen et al., 1999; Denton et al., 1999; Glasser et al., 2008; Moreno et al., 2015; Kilian and Lamy, 2012; Lamy et al., 2010), and have served as important constraints towards understanding the drivers of ice sheet change across centennial to millennial timescales. Currently, PATICE (Davies et al., 2020) serves as the latest and most complete reconstruction of the entire PIS during the LGM and last deglaciation. Across the CLD (Figure 1), the LGM ice limits are well constrained by terminal moraines in the southwest and western margins (Denton et al., 1999; Glasser et al., 2008; Moreno et al., 2015). However, due to a lack of geomorphological and geochronologic constraints on past ice margin change, the reconstructed deglaciation remains highly uncertain.

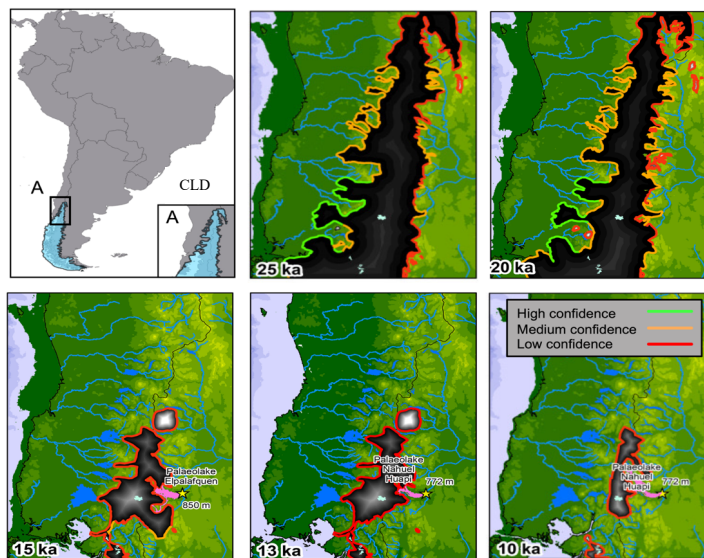


Figure 1. Location of the study area across the Chilean Lake District (CLD; Upper Left Panel). The reconstructed ice extent from PATICE for the PIS across the CLD at 25 ka, 20 ka, 15 ka, 13 ka, and 10 ka are taken from Davies et al., 2020. The color of the line marking the reconstructed ice extent corresponds to the confidence in the reconstruction as described in section 3.3.

While deglacial warming is a primary driver of ice retreat across the CLD, evidence suggests that variations in precipitation patterns influenced the timing and magnitude of this retreat (Moreno et al., 1999; Rojas et al., 2009). The wintertime climate across South America is strongly influenced by the southern westerly winds (SWW), which exert a large control on the synoptic scale hydrologic and heat budget (Garreaud et al., 2013). During the LGM and last deglaciation,

Deleted: ¶

Deleted: an area along

Deleted: ; 2015

Deleted: last glacial

102 paleoclimate data indicates that the position, strength, and extent of the SWW varied latitudinally,
103 migrating southward during warmer intervals and northward during cooler intervals, ultimately
104 altering overall ice sheet mass balance (Mercer, 1972; Denton et al., 1999; Lamy et al., 2010;
105 Kilian and Lamy, 2012; Boex et al., 2013). Terrestrial paleoclimate proxies that indicate that the
106 CLD was wetter during the LGM and early deglaciation have been used to support the idea that
107 the SWW migrated northward of 41°S across the CLD (Moreno et al., 1999; Moreno et al., 2015;
108 Moreno and Videla, 2018; Diaz et al., 2023). Additionally, these proxies indicate a switch from
109 hyper humid to humid conditions around 17,300 cal yr BP, which was inferred by Moreno et al.
110 (2015) to indicate the poleward migration of the SWW south of the CLD.

111
112 However, inferring changes in the SWW across the last deglaciation from paleoclimate proxies
113 can be problematic as outlined by Kohfeld et al. (2013) who compiled an extensive dataset of
114 paleoclimate archives that record changes in moisture, precipitation-*evaporation balance*, ice
115 accumulation, runoff and precipitation, dust deposition, and marine indicators of sea surface
116 temperature, ocean fronts, and biologic productivity. Kohfeld et al. (2013) conclude that
117 environmental changes inferred from existing paleoclimate data could be potentially explained by
118 a range of plausible scenarios for the state and change of the SWW during the LGM and last
119 deglaciation, such as a strengthening, poleward or equatorward migration, or no change. Climate
120 model results from Sime et al. (2013) indicate that the reconstructed changes in moisture from
121 Kohfeld et al. (2013) can be simulated well without invoking large shifts or changes in strength to
122 the SWW. This discrepancy also exists amongst climate models which diverge on whether the
123 LGM SWW was shifted equatorward or poleward, and was stronger or weaker than present day
124 (Togweiler et al., 2006; Menviel et al., 2008; Rojas et al., 2009; Rojas et al., 2013; Sime et al.,
125 2013; Jiang et al., 2020). Therefore, from paleoclimate proxies and climate models, we still do
126 not have a firm understanding of how the SWW may have changed during the last deglaciation,
127 and how these variations may have influenced the deglaciation of the PIS.

128
129 Early paleo ice sheet modelling experiments across the PIS have focused on evaluating the
130 relationship between the simulated LGM ice sheet geometry in response to spatially uniform
131 temperature change (Hulton et al., 2002; Sugden et al., 2002; Hubbard et al., 2005). While these
132 early simulations provided constraints on PIS areal extent, ice volume, and sensitivity to LGM
133 temperature depressions, spatially varying temperature and precipitation were not considered.
134 Recently, Yan et al. (2022) simulated the PIS behavior at the LGM using an ensemble of climate
135 model output from the Paleoclimate Modelling Intercomparison Project (PMIP4; Kageyama et al.,
136 2021). Results best matching the empirical reconstructions from PATICE (Davies et al., 2020)
137 suggest that reduction in temperature was likely the main driver of PIS LGM extent, although the
138 authors found that variation in regional LGM precipitation anomaly can have large impacts on the
139 simulated ice sheet geometry. This evidence is supported by recent glacier modelling across the
140 northeastern Patagonian Andes which suggests that increases in precipitation during the
141 termination of the LGM are necessary to achieve modeled fit with reconstructed glacier extent
142 (Muir et al., 2023; Leger et al., 2021). Additionally, Martin et al. (2022) found that precipitation
143 greater than present day are needed to explain late glacial and Holocene ice readvance of the Monte
144 San Lorenzo ice cap, lying to the southeast of the current Northern Patagonian Ice Field. These
145 regional studies therefore provide further evidence that late glacial and deglacial variability in
146 precipitation, perhaps driven by changes in the SWW, influenced PIS retreat and readvance over
147 numerous timescales.

Deleted: strongly influenced by a shifting SWW position during the last deglaciation

Deleted: 6

Deleted: hyperhumid

Deleted: we note that

Deleted: in the SWW

Deleted: proxy records

Deleted: precipitataan

Deleted: in the SWW

Deleted:

Deleted: ¶

¶

¶ However, due to limitations in the spatial abundance and resolution of these paleoclimate proxies (Kohfeld et al., 2013), as well as certainty in deglacial ice sheet reconstructions (see Figure 1), assessment of the climatic drivers of past ice sheet change across this region remains difficult. ¶

Deleted: climate

Deleted: the SWW

169 To advance our understanding of the last glacial and deglacial ice behavior across the CLD, we
170 use a numerical ice sheet model to simulate the LGM ice geometry and deglacial ice retreat using
171 transiently evolving boundary conditions from a climate model simulation of the last 21,000 years
172 (TraCE-21ka; Liu et al., 2009; He et al., 2013) which simulates large scale variability in the
173 strength and position of the SWW (Jiang and Yan, 2020). Because there is a lack of transiently
174 evolving ice sheet model simulations of the PIS across the last deglaciation, our aim is to provide
175 possible constraints on the nature of ice retreat across the CLD region, from which the
176 reconstructions (PATICE; Davies et al., 2020) are uncertain. Also, by assessing the sensitivity of
177 our ice sheet experiments to a range of climatic boundary conditions, we aim to provide additional
178 insight into the dominant climatic controls on the deglacial evolution of the PIS in the CLD region.
179

- Deleted: ¶
- Deleted: use the Ice Sheet and Sea-level System Model (ISSM; Larour et al., 2012) to
- Deleted: first
- Deleted: forced by an ensemble of climate boundary conditions from PMIP4 models (Kageyama et al., 2021). Second, we simulate the
- Deleted: evolution of the PIS across the CLD

180 2 Methods: Model description and setup

- Deleted: ¶

182 2.1 Ice sheet model

184 In order to simulate the ice margin migration across the CLD during the LGM and last deglaciation,
185 we use the Ice Sheet and Sea-level System Model (ISSM), a thermomechanical finite-element ice
186 sheet model (Larour et al., 2012). Because of the high topographic relief across the CLD and
187 associated impact on ice flow, we use a higher-order approximation to solve the momentum
188 balance equations (Dias dos Santos et al., 2022). This ice flow approximation is a depth-integrated
189 formulation of the higher-order approximation of Blatter (1995) and Pattyn (2003), which allows
190 for an improved representation of ice flow compared with more traditional approaches in paleo-
191 ice flow modelling (e.g., Shallow Ice Approximation or hybrid approaches; Hubbard et al., 2005;
192 Leger et al., 2022; Yan et al., 2022), while allowing for reasonable computational efficiency. Our
193 model domain comprises the northernmost LGM extent of the PIS across the CLD, extending
194 beyond the LGM ice extent reconstructed from Davies et al. (2020) and ends along the northern
195 shore of the Golfo de Ancud (Figure 2).
196

- Deleted: extent

197 We rely on anisotropic mesh adaptation to create a non-uniform model mesh that varies based
198 upon gradients in bedrock topography from the General Bathymetric Chart of the Oceans
199 (GEBCO; GEBCO Bathymetric Compilation Group, 2021), a terrain model for ocean and land.
200 For the land component, the GEBCO model uses version 2.2 of the Surface Radar Topography
201 Mission data (SRTM15_plus; Tozer et al., 2019), to create a 15 arc second gridded output of terrain
202 elevation relative to sea level. Our ice sheet model horizontal mesh resolution varies from 3 km
203 in areas of low bedrock relief to 450 meters in areas where gradients in the bedrock topography is
204 high and comprises 40,000 model elements.
205
206

- Deleted:

- Deleted: of

- Deleted: ¶

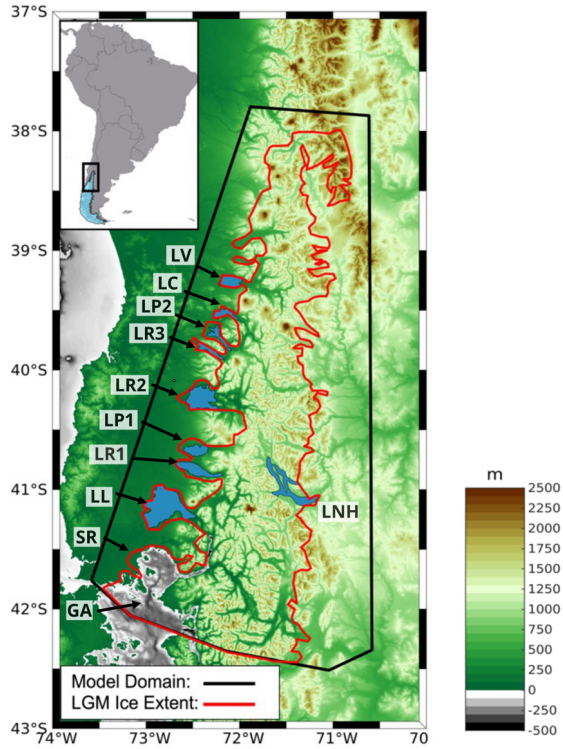


Figure 2. Bedrock topography for our study area (meters). Our model domain (shown as the black line), encompasses the reconstructed LGM ice limit (shown in red) from PATICE (Davies et al., 2020). Present day lakes are shown in blue, with abbreviated names as: SR (Seno de Reloncaví), GA (Golfo de Ancud), LL (Lago Llanquihue), LR1 (Lago Rupanco), LP1 (Lago Puyehue), LR2 (Lago Ranco), LR3 (Lago Riñihue), LP2 (Lago Panguipulli), LC (Lago Calafquén), LV (Lago Villarica), LNH (Lago Nahuel Huapi).

Although geomorphological evidence suggests that while southernmost glaciers across the PIS may have been temperate with warm based conditions during the LGM, there may have been periods where ice lobes were polythermal (Darvill et al., 2016). However, recent ice flow modelling (Leger et al., 2021) suggests that varying ice viscosity mainly impacts the accumulation zone thickness in simulations of paleoglaciers in Northeastern Patagonia, with minimal impacts on overall glacier length and extent. Accordingly, based on sensitivity tests (see supplement section S1), our model is 2-dimensional and we do not solve for ice temperature and viscosity allowing for increased computational efficiency. For our purposes, we use Glen's flow law (Glen, 1955) and set the ice viscosity following the rate factors in Cuffey and Paterson (2010) assuming an ice temperature of -0.2°C . We use a linear friction law (Budd et al., 1979)

$$\tau_b = -k^2 N v_b \quad (1)$$

Formatted: Font: (Default) Times New Roman, 10 pt

Formatted: Caption, Left

Deleted: ¶

Formatted: Font color: Text 1

Commented [JC2]: Make sure to cite proper section of supplement

Formatted: Font color: Text 1

Formatted: Font color: Text 1

Deleted: Although geomorphological evidence suggests that while southernmost glaciers across the PIS may have been temperate with warm based conditions during the LGM, there may have been periods where ice lobes were polythermal (Darvill et al., 2016). Although evidence suggests that while southernmost glaciers across the PIS may have been polythermal, data suggests that the majority of the PIS was temperate (isothermal). Accordingly, recent ice flow modelling (Leger et al., 2021) suggests that varying ice viscosity mainly impacts the accumulation zone thickness in simulations of paleoglaciers in Northeastern Patagonia, with minimal impacts on overall glacier length and extent. Therefore, our model is 2-dimensional and we do not solve for ice temperature and viscosity allowing for increased computational efficiency.

Formatted: Font color: Text 1

Formatted: Font color: Text 1

Formatted: Font color: Blue

Formatted: Font color: Text 1

248
249
250
251
252
253
254
255
256
257
258
259
260
261
262
263
264
265
266
267
268
269
270
271
272
273
274
275
276
277
278
279
281
282
283
284
285
286
287
288
289
290
291

where τ_b represents the basal stress, N represents the effective pressure, and v_b is the magnitude of the basal velocity. Here $N = g(\rho_i H + \rho_w Z_b)$, where g is gravity, H is ice thickness, ρ_i is the density of ice, ρ_w is the density of water, and Z_b is bedrock elevation following Cuffey and Paterson (2010).

The spatially varying friction coefficient, k , is constructed following Åkesson et al. (2018):

$$k = 200 \times \frac{\min(\max(0, z_b + 600), z_b)}{\max(z_b)} \quad (2)$$

where z_b is the height of the bedrock with respect to sea level. Using this parameterization, basal friction is larger across high topographic relief and lower across valleys, and areas below sea level.

To account for the influence of glacial isostatic adjustment (GIA), we prescribe a transiently evolving reconstruction of relative sea level from the global GIA model of the last glacial cycle from Caron et al. (2018). This includes three physical components: 1) Bedrock vertical motion 2.) Eustatic sea level, and 3.) Geoid changes. The time series we use to prescribe GIA is from the model average of an ensemble of GIA forward model estimations from Caron et al., 2018. The prescribed GIA is in good agreement (Figure S2) with a reconstruction of relative sea-level change from an isolation basin in central Patagonia (Troch et al., 2022). This methodology has been applied in recent modelling following Cuzzone et al. (2019) and Briner et al. (2020).

2.2 Experimental Design

In order to simulate the ice history at the LGM and across the last deglaciation we use climate model output from the National Center for Atmospheric Research Community Climate System Model (CCSM3) TraCE-21ka transient climate simulation of the last deglaciation (Liu et al., 2009; He et al., 2013). Monthly mean output of temperature and precipitation are used from these simulations as inputs to our glaciological model (full climate forcings details are further described in section 2.4) and we use the monthly mean output every 50 years across the last deglaciation. Large, multi-proxy reconstructions from He and Clark (2022), Liu et al. (2009), He et al. (2011), and Shakun et al. (2012; 2015) have all demonstrated good agreement between TRACE 21k and a wide variety of paleo-proxy data during the last deglaciation that include records from the West Antarctic and South America.

2.3 Surface Mass Balance

In order to simulate the deglaciation of the PIS across our model domain we require inputs of temperature and precipitation to estimate the surface mass balance. To derive snow and ice melt we use a positive degree day model (Tarasov and Peltier, 1999; Le Morzadec et al., 2015; Cuzzone et al., 2019; Briner et al., 2020). Our degree day factor for snow melt is $3 \text{ mm } ^\circ\text{C}^{-1}\text{day}^{-1}$ and $6 \text{ mm } ^\circ\text{C}^{-1}\text{day}^{-1}$ for bare ice melt, and we use a lapse rate of $6 \text{ }^\circ\text{C}/\text{km}$ to adjust the temperature of the climate forcings to surface elevation, which are within a range of typical values used to model contemporary and paleo glaciers across Patagonia (see Fernandez et al., 2016 Table 3; Yan et al., 2022). The hourly temperatures are assumed to have a normal distribution, of standard deviation 3.5 degrees Celsius around the monthly mean. An elevation-dependent desertification

- Formatted: Subscript
- Formatted: Font color: Text 1
- Deleted: ¶
- Formatted: Font color: Text 1
- Formatted: Space After: 11.7 pt
- Formatted: Font color: Text 1
- Deleted: 1
- Deleted: To account for the influence of glacial isostatic adjustment (GIA), we prescribe a transiently evolving reconstruction of relative sea level from the global GIA model of the last glacial cycle from Caron et al. (2018). This includes 3 physical components: 1) Bedrock vertical motion 2.) Eustatic sea level, and 3.) Geoid changes.¶
- Formatted: Pattern: Clear
- Deleted: ¶
- Currently ISSM is undergoing model developments to include a full treatment of solid earth-ice and sea-level feedbacks (Adhikari et al., 2016). Therefore, at this time, there is no interaction between our simulated ice sheet and the solid earth. We do however account for changes in the geoid at the LGM and across the last deglaciation using a time dependent forcing from Caron et al. (2018) that accounts for relative sea-level changes following setups in Briner et al. (2020) and Cuzzone et al. (2019). ¶
- Deleted: ¶
- Formatted: Space After: Auto
- Moved up [3]: Monthly mean output of temperature and precipitation at varying horizontal resolution (Table 1) are used from these simulations as inputs to our glaciological model (full climate forcings details are further described in section 2.4). ¶
- Moved (insertion) [3]
- Deleted: Monthly mean output of temperature and ... [1]
- Deleted:
- Deleted: We perform simulations of a.) the LGM ... [2]
- Deleted: Table 1. List of model output used for the cli ... [3]
- Deleted: ¶
- Deleted: Simulation across the last deglaciation: In or ... [4]
- Deleted: ¶ ... [5]
- Moved (insertion) [2]
- Deleted: are
- Deleted: of those
- Deleted: ¶ ... [6]
- Formatted ... [7]
- Formatted: Font color: Text 1
- Formatted ... [8]

is included (Budd and Smith, 1981) which reduces precipitation by a factor of 2 for every kilometer change in ice sheet surface elevation. We note that the values in the surface mass balance parameters were chosen to provide a reasonable fit within 5% between the simulated LGM ice sheet area and the reconstructed ice area from PATICE (see Figure 10).

2.4 Climate forcings

In order to scale monthly temperature and precipitation across the LGM and last deglaciation we applied a commonly used modeling approach (Pollard et al., 2012; Seguinot et al., 2016; Golledge et al., 2017; Tigchelaar et al., 2019; Clark et al., 2020; Briner et al., 2020; Cuzzone et al., 2022; Yan et al., 2022; equations 3 and 4). First, we use the monthly mean climatology of temperature and precipitation for the period 1979-2018 ($T_{(1979-2018)}$, $P_{(1979-2018)}$) from the Center for Climate Resilience Research Meteorological dataset version 2.0 (CR2MET; Boisier et al., 2018). This output, which uses information from a climate reanalysis and is calibrated against rain-gauge observations, is provided at 5 km spatial resolution. We then bilinearly interpolate these fields onto our model mesh.

$$T_t = T_{(1979-2018)} + \Delta T_t \quad (3)$$

$$P_t = P_{(1979-2018)} + \Delta P_t \quad (4)$$

Next, anomalies of the monthly temperature and precipitation fields are computed as the difference from the preindustrial control run and interpolated onto our model mesh (ΔT_t and ΔP_t). These anomalies are added to the contemporary monthly mean as shown in equations 3 and 4, to produce the monthly temperature and precipitation fields at LGM and across the last deglaciation (T_t and P_t).

2.5 Ice front migration and iceberg calving

We simulate calving where the PIS interacts with ocean. We track the motion of the ice front using the level-set method described in Bondzio et al. (2016; equation 3) in which the ice velocity (v_f) is a function of the ice velocity vector at the ice front (v), the calving rate (c), the melting rate at the calving front (M), and where n is the unit normal vector pointing horizontally outward from the calving front. For these simulations the melting rate is assumed to be negligible compared to the calving rate, so M is set to 0.

$$v_f = v - (c + M) n \quad (5)$$

To simulate calving we employ the more physically based Von Mises stress calving approach (Morlighem et al., 2016) which relates the calving rate (c) to the tensile stresses simulated within the ice, where σ is the von Mises tensile strength, $\|v\|$ is the magnitude of the horizontal ice velocity, and σ_{max} is the maximum stress threshold which has separate values for grounded and floating ice.

$$c = \|v\| \frac{\sigma}{\sigma_{max}} \quad (6)$$

Deleted: ctio

Deleted: n in

Formatted: Font color: Text 1

Formatted: Font color: Text 1

Deleted: (Budd and Smith, 1981)..

Deleted: Using these parameter values,

Deleted: These

Formatted: Font color: Text 1

Deleted: we arrive at a

Moved up [2]: are typical of those used to model contemporary and paleo glaciers across Patagonia (see Fernandez et al., 2016 Table 3; Yan et al., 2022).

Deleted: that

Deleted: These values are typical of those used to model contemporary and paleo glaciers across Patagonia (see Fernandez et al., 2016 Table 3; Yan et al., 2022).

Deleted: each model's

Deleted: Therefore, LGM anomalies for each model are computed as well as anomalies across the last deglaciation (Liu et al., 2009; He et al., 2013).

Deleted: ¶

Moved down [1]: Across most of our domain, there is evidence for an advance of piedmont glaciers across glacial outwash during the LGM, which formed the physical boundary for some of the existing terminal moraines around the lakes within the CLD (Bentley, 1996; Bentley, 1997). Where there were proglacial lakes along the westward ice front in the CLD, evidence suggests that ice was grounded during the LGM (Lago Puyehue; Heirman et al., 2011). During deglaciation, iceberg calving into the proglacial lakes may have occurred (Davies et al., 2020), with evidence suggesting that local topography and calving may have controlled the spatially irregular timing of abandonment from the terminal moraines surrounding the proglacial lakes (Bentley, 1997). However, because inclusion of ice-lake interactions is relatively novel for numerical ice flow modeling (Sutherland et al., 2020; Quiquet et al., 2021; Hinck et al., 2022), we choose to not model the evolution and influence of proglacial lakes on the deglaciation across this model domain. Instead, we only simulate calving where the PIS interacts with the ocean.

Deleted: ¶

Deleted: (

451
452
453
454
455
456
457
458
459
460
461
462
463
464
465
466

The ice front will retreat if von Mises tensile strength exceeds a user defined stress threshold, which we set to 200 kPa for floating ice and 1 MPa for tidewater ice. This calving law has been applied in Greenland to assess marine terminating icefront stability (Bondzio et al., 2016; Morlighem et al., 2016; Choi et al., 2021; Cuzzone et al., 2022) and for our simulations applies where ocean is present such as the Seno de Reloncaví and the Golfo de Ancud (see Figure 2).

3 Results

3.1 Simulated LGM state

In order to arrive at a steady state LGM ice geometry, we first initialize our model with an ice-free configuration. A constant LGM monthly climatology of temperature and precipitation are then applied, as well as the prescribed GIA from Caron et al. (2018). We allow the ice sheet to relax for 10,000 years, during which, the ice sheet is free to grow and expand until it reaches a steady state ice geometry and volume, in equilibrium with the climate forcings.

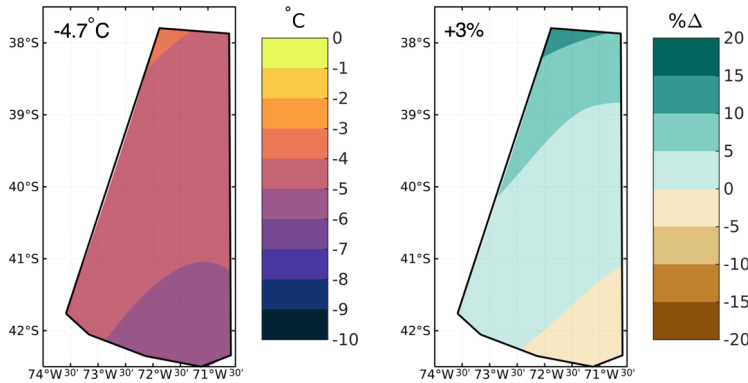


Figure 3. The LGM summer (DJF) temperature anomaly (left panel) and the LGM winter precipitation anomaly (right panel) from TraCE-21ka. Anomalies are taken as the difference between the LGM and preindustrial (LGM-PI), with the precipitation anomalies expressed as the percent difference of the LGM from preindustrial. The area averaged value of the anomaly is shown in the upper left of each panel.

467
468
469
470
471
472
473
474

At 22 ka, Trace-21ka simulates an area averaged summertime (DJF) cooling of 4.7°C relative to the PI across our model domain (Figure 3). The LGM cooling increases from north to south, with the greatest magnitude of cooling occurring across the southern portion of our model domain of up to 6°C. During winter (JJA), Trace-21ka simulates an overall wetter climate across our model domain during the LGM relative to the PI. While the area-averaged LGM precipitation anomaly is small (3% higher), the LGM precipitation anomaly increases from south to north, with Trace-21ka simulating 10-15% more wintertime precipitation during the LGM than the PI across the

Deleted: grounded ice

Deleted: LGM Experiments

Formatted: Right: 0"

Deleted: The

Deleted: LGM geoid

Deleted: These relaxation steps are performed for the separate experiments using the individual climate model output described in section 2.2.

Formatted: Caption, Left

482 northern portion of the model domain. While the mean position of the wintertime SWW is
 483 simulated to be poleward during the LGM relative to the PI in TraCE-21ka (Jiang and Yan, 2022),
 484 the low-level zonal wind (925 hPa) is stronger during the LGM across our model domain and
 485 Patagonia (Figure S3A). We also find that relative to PI, wintertime lower level (850 hPa)
 486 moisture flux convergence is higher during the LGM across our model domain (Figure S4A).
 487

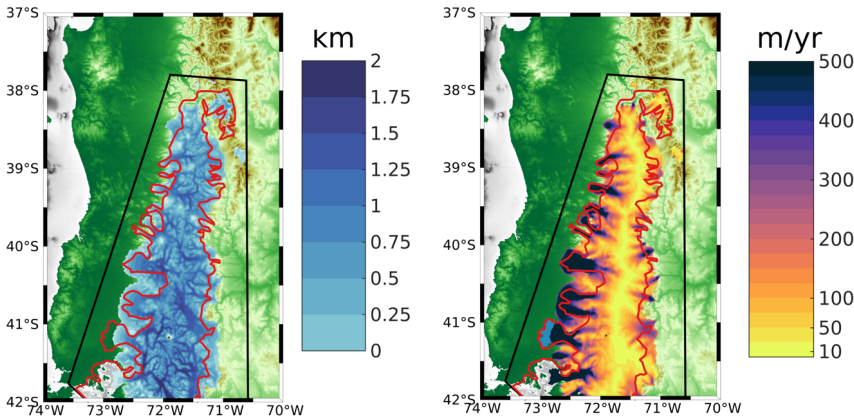


Figure 4. The simulated LGM ice thickness (km; left panel) and the simulated LGM ice surface velocity (km/yr; right panel) is shown. The black outline denotes our ice sheet model boundary, and the red line denotes the LGM reconstructed ice extent from PATICE (Davies et al., 2020).

488 Bedrock elevation increases from west to east, with deep valleys interspersed across most of our
 489 model domain (Figure 2). Consistent across all simulations, ice thickness is greatest in these
 490 valleys (upwards of 2000 meters) where driving stresses dominate and where bedrock geometry
 491 controls the flow of ice from higher terrain and through these valleys. Across the highest terrain
 492 such as the many volcanoes across the CLD, ice is comparatively thinner than the surrounding
 493 valleys. An ice divide is present as slow ice velocities in the interior of the ice sheet, which give
 494 way to fast flowing outlet glaciers especially on the western margin of the CLD where velocities
 495 reach in excess of 500 m/yr and in some location up to 2 km/yr. The simulated LGM ice sheet
 496 area across the CLD is 414,120 km², which is within 1% of the area calculated from the PATICE
 497 reconstruction (414,690 km²). This agreement is in part due to the tuning of our degree day factors
 498 as discussed in section 2.3, and gives confidence to our ability to simulate a reasonable LGM ice
 499 sheet across the CLD and throughout the last deglaciation.

501 3.2 Simulation of the Last Deglaciation

502
 503 Monthly mean temperature and precipitation, taken every 50 years from the TraCE-21ka (Liu et
 504 al., 2009; He et al., 2013) experiment is used to drive our simulation of ice history across the last
 505 deglaciation (22 ka – 10 ka). The transient simulation is initialized with the LGM ice sheet
 506 geometry shown in Figure 4, and is run forward with the appropriate climate boundary conditions
 507 until 10 ka.

Deleted: <object>

Formatted: Justified

Formatted: Caption, Left

Moved up [4]: Across our model domain, bedrock elevation increases from west to east, with deep valleys interspersed across most of our model domain (Figure 2). Consistent across all simulations, ice thickness is greatest in these valleys (upwards of 2000 meters) where driving stresses dominate and where bedrock geometry controls the flow of ice from higher terrain and through these valleys (Figure 5).

Moved (insertion) [4]

Deleted: In Figure 4 is the simulated LGM ice thickness and ice surface velocities across our model domain, with the red outline indicating the reconstructed LGM ice extent (20 ka) from PATICE (Davies et al., 2020). Across our model domain, bedrock elevation increases from west to east, with deep valleys interspersed across most of our model domain (Figure 2). Consistent across all simulations, ice thickness is greatest in these valleys (upwards of 2000 meters) where driving stresses dominate and where bedrock geometry controls the flow of ice from higher terrain and through these valleys (Figure 5). Across the highest terrain, such as the many volcanoes across the CLD, ice is comparatively thinner than the surrounding valleys. An ice divide is present as slow ice velocities in the interior of the ice sheet, which give way to fast flowing outlet glaciers especially on the western margin of the CLD where velocities reach in excess of 500 m/yr and in some location up to 2 km/yr. The simulated LGM ice sheet area across the CLD is 4.1412e4 km², which is within 1% of the area calculated from the PATICE reconstruction (4.1469e4). This agreement is in part due to the tuning of our degree day factors as discussed in section 2.3, and gives confidence to our ability to simulate a reasonable LGM ice sheet across the CLD and throughout the last deglaciation.

Deleted: ¶

3.1.1 LGM climate ¶

<object>Shown in Figures 3 are the anomalies (LGM-preindustrial) of summer temperature (DJF) and winter precipitation (JJA) for each climate model. The area averaged anomaly is shown in the upper lefthand corner of each sub figure. In general, the climate models simulate an LGM climate that is colder than preindustrial, with summer temperature anomalies ranging between -4.7°C (TraCE-21ka) to -7.9°C (MPI). Generally, the climate models exhibit larger cooling during the LGM compared to the preindustrial over the central to southern portions of our model domain, although the magnitude of those changes...

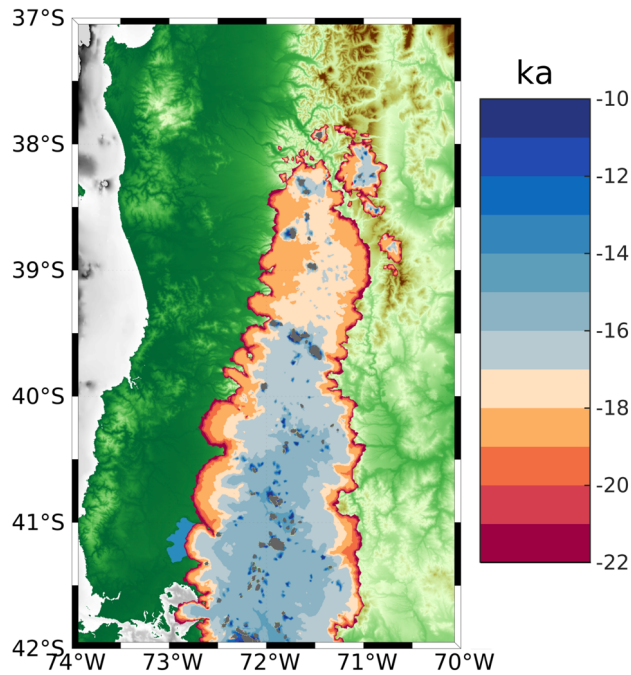
Deleted: ¶

3.1.3 LGM ice extent and sensitivity to climate ¶

<object>The resulting ice volume across our model domain is plotted against the LGM anomaly of summer temperature and winter precipitation in Figure 6. Model simulations...

Deleted: 4 (TraCE-21ka)

690 3.2.1 Pattern of Deglaciation



717 Figure 5. The simulated deglaciation age for the transient simulation from the LGM to 10 ka. The gray color indicates where ice persists after 10 ka.

720 From the resulting transient simulation, we calculate the timing of deglaciation across our model domain (Figure 5). Because of possible readvances during the deglaciation, we select the youngest age at which grid points become ice free. Our map of the simulated deglaciation can be paired with a timeseries of the rate of ice mass change (Figure 6, bottom panel) to highlight some key features in the magnitude and timing of ice retreat between 22 ka and 10 ka.

726 Between 22 ka to 19 ka, the ice sheet undergoes periods of minor to moderate ice mass loss and gain in an interval of time where summer temperature anomalies (Figure 6) and the corresponding ice margin remain relatively stable (Figure 5). Between 19 ka and 18.5 ka, coincident with a rise in summertime temperature (Figure 6), a pulse of ice mass loss exceeding 5,000 GT/century occurs before trending toward minimal ice mass loss around 18 ka as the rise in summer temperature levels off. During this time interval, the ice margin pulls back considerably towards higher terrain across the northern portion of the model domain (Figure 5), and many of the fast-flowing outlet glaciers on the western margin retreat back towards the ice sheet interior. Between 18 ka to 16.2 ka, summer temperature rises steadily ~1.2°C and is punctuated with an abrupt warming of ~0.5°C at 16 ka (Figure 6). During this interval, ice mass loss remains high and steady at ~1000

Deleted: ¶

Formatted: Caption

Deleted: 7A

Deleted: 8

739 GT/century with pulses of increased mass loss at 17.8 ka, 16.8 ka, and 16 ka varying between
 740 2000-5000 GT/century (Figure 6).
 741

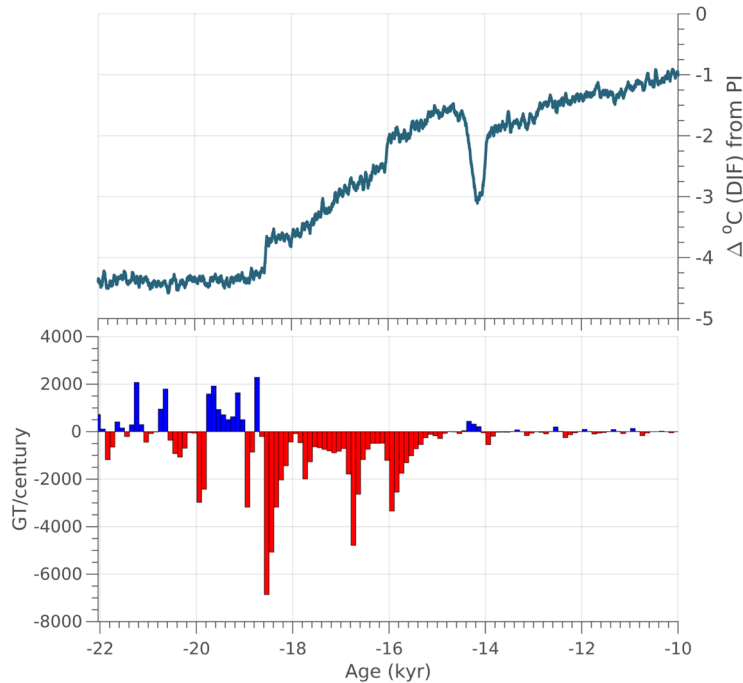


Figure 6. Top Panel: The TraCE-21ka Summer (DJF) temperature anomaly taken as the difference from the preindustrial period, area averaged across our model domain. Bottom Panel: The simulated ice mass change calculated in GT/century across the last deglaciation (22 ka to 10 ka). Red indicates ice mass loss, and blue indicates ice mass gain.

742
 743 By 17 ka, the northern portion of the model domain (north of 39.5°S), has generally become ice
 744 free for the exception of the highest terrain (e.g., mountain glaciers). By 16 ka, between 39.5°S
 745 and 40.5°S, ice remains only on the highest terrain (Figure 5), however ice cover persists south of
 746 40.5°S. Between 16 ka and 15 ka, summer temperature rises ~0.5°C (Figure 6) and the remaining
 747 ice sheet retreats south of 40.5°S. By 15 ka, there is no evidence of an ice sheet, with only
 748 mountain glaciers and small ice caps (eg. Cerro Tronador) existing across the high terrain
 749 throughout the model domain (Figure 5).

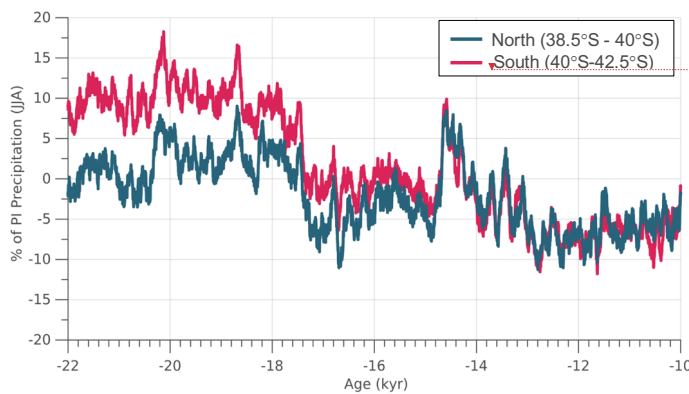
750
 751 After 15 ka, TraCE-21ka simulates a short and abrupt Antarctic Cold Reversal (ACR) between
 752 14.6 ka and 14 ka (Figure 6), before temperatures continue to rise into the early Holocene. There
 753 is only a minor ice mass gain (e.g., <500 GT/yr) during the ACR, and minimal fluctuation in ice
 754 mass after 14 ka. By 10 ka, only small mountain glaciers persist across the high terrain and
 755 volcanoes of the CLD (gray color in Figure 5).

- Deleted: ¶
- Formatted: Caption, Left
- Deleted: <object><object>¶
- Between 22 ka to 19 ka, the ice sheet undergoes periods of minor to moderate ice mass loss and gain (Figure 8), in an interval of time where summer temperature anomalies and the corresponding ice margin remain relatively stable (Figure 7a). Between 19 ka and 18.5 ka, coincident with a rise in summertime temperature (Figure 8), a pulse of ice mass loss occurs and exceeds 5,000 GT/century before trending toward minimal ice mass loss around 18 ka as the rise in summer temperature levels off. During this time interval, the ice margin pulls back considerably towards higher terrain across the northern portion of the model domain (Figure 7A), and many of the fast-flowing outlet glaciers on the western margin retreat back towards the ice sheet interior. Between 18 ka to 16.2 ka, summer temperature rises steadily ~1.2°C and is punctuated with an abrupt warming of ~0.5°C at 16 ka (Figure 8). During this interval, ice mass loss remains high and steady at ~1000 GT/century with pulses of increased mass loss at 17.8 ka, 16.8 ka, and 16 ka varying between 2000-5000 GT/century (Figure 8). ¶
- Deleted: and
- Deleted: 7A
- Deleted: 8
- Deleted: 7A
- Deleted: <object>
- Deleted: 8
- Deleted: 7

785 3.2.2 Sensitivity Test

786 To better assess how changes in precipitation may modulate the deglaciation across the CLD we
787 perform additional sensitivity tests. We refer to the simulation discussed above as our main
788 simulation, where the climate boundary conditions of temperature and precipitation varied
789 temporally and spatially across the last deglaciation. Three more simulations are performed where
790 temperature is allowed to vary across the last deglaciation, but precipitation remains fixed at a
791 given magnitude for a particular time interval. Each experiment is listed below as:
792

- 793 1) Monthly precipitation is held constant at the preindustrial mean. In Figure 7, preindustrial
794 precipitation is reduced compared to the period 22 ka to 18 ka, but is similar to and higher
795 than what is simulated after 18 ka for the exception of the ACR at 14.5 ka.
- 796 2) Monthly precipitation is held constant at the 12.5 ka-12 ka mean. This is a period of
797 reduced precipitation relative to the preindustrial (~7% reduction; Figure 7).
- 798 3) Monthly precipitation is held constant to the 22-20 ka mean, which is approximately 10%
799 higher than preindustrial values across the Northern portion of the model domain (North
800 of 40°S).



801 Figure 7. The winter (JJA) precipitation anomaly expressed as the percent difference from the preindustrial period.
802 The area averaged anomaly is shown for the region north of 40°S and for the region south of 40°S (see Figure 2 for
803 reference to the latitudinal range of our model domain).

804 Across our model domain during experiment 2 (Figure 8A), wintertime precipitation during the
805 preindustrial is reduced compared to the early deglaciation (22 ka to 18ka) and is similar to slightly
806 higher particularly south of 40°S after 18 ka (Figure 7). When holding precipitation constant at
807 the preindustrial mean through the last deglaciation, the ice retreats faster across most portions of
808 the model domain, particularly along the ice margins and in area north of 40°S. In the southern
809 portion of our model domain (south of 40°S), where the changes in deglacial precipitation relative
810 to the preindustrial are lower (Figure 7), the difference in simulated deglaciation age are also
smaller. In general, the pace of deglaciation increases by up to 1 kyr compared to the main
simulation, with many locations experiencing deglaciation 200-600 yrs earlier than the main
simulation.

Formatted: Font color: Text 1

Formatted: Font color: Text 1

Formatted: Font color: Text 1

Formatted: Font color: Text 1

Formatted: Font color: Text 1

Deleted:

Formatted: Caption, Space After: 0 pt, No bullets or numbering

Deleted: In Figure 8A, the difference in the deglaciation age between sensitivity experiment 1 and the main simulation is shown, where precipitation is held constant at the preindustrial monthly mean.

Formatted: Font color: Text 1

Formatted: Font color: Text 1

Formatted: Font color: Text 1

Deleted: we notice that

Formatted: Font color: Text 1

Formatted: Font color: Text 1

Formatted: Font color: Text 1

Formatted: Font color: Text 1

Formatted: Font color: Text 1

816

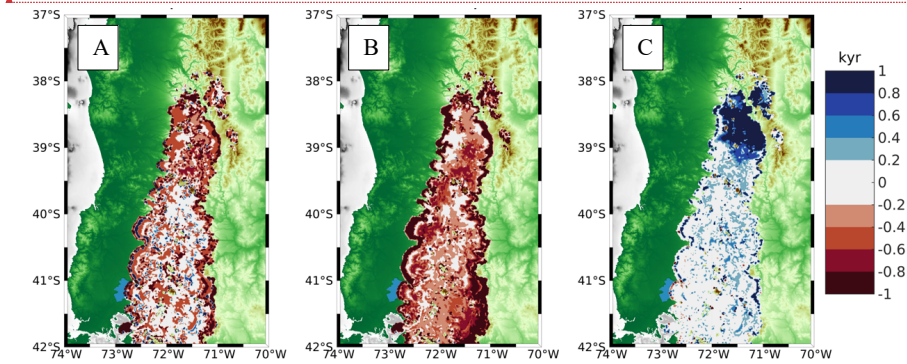


Figure 8. A) The difference in the simulated deglaciation age between sensitivity experiment 2, B.) experiment 3, C.) and experiment 4, from the main simulation. Blue colors indicate slower ice retreat for the sensitivity experiments compared to the main simulation, while red colors indicate faster ice retreat for the sensitivity experiments compared to the main run.

For our other two sensitivity tests, winter precipitation is reduced by up to 7% (Figure 8B) relative to the preindustrial across the model domain (Figure 7) and increased by up to 10% (Figure 8C) across the northern portion of the model domain (north of 40°S), but is similar to preindustrial values across the southern portion of our model domain (south of 40°S). For experiment 2 ice retreats faster across most of the CLD, along the ice margins and through the interior. Deglaciation along the margins occurs >1 kyr faster in many locations, and between 200 yrs to 1 kyr faster across portions of the ice interior. In experiment 3 with the imposed higher precipitation across the northern portion of the model domain, ice retreats slower during the last deglaciation relative to our standard simulation by >1 kyr, and in some locations up to 2 kyr.

3.3 Comparison to the reconstructed deglacial ice extent

Shown in Figure 1, PATICE assigns high to medium confidence to the reconstructed LGM (25 ka ± 20 ka) ice extent along most of the western ice margin and portions of the eastern margin, with low confidence assigned to the northernmost ice extent. The majority of the ice history is poorly constrained (low confidence) during the deglaciation, and PATICE reconstructs a small cap that persists across the southern CLD until 10 ka, after which the ice disappears and only the Cerro Tronador glacier remains (see Figure 13 from Davies et al., 2020). We show the simulated and reconstructed ice extent in Figure 9 as well as the calculated ice area from PATICE at 20 ka, 15 ka, 13 ka, and 10ka and for our transient simulation in Figure 10. At 22 ka (Figure 9), our model simulates a generally greater ice extent along the eastern and western margin, except at the Seno de Reloncaví, Golfo de Ancud, and Lago Llanquihue, where the simulated ice margin does not advance to the well dated terminal LGM moraines (Mercer, 1972; Porter, 1981; Andersen et al., 1999; Denton et al., 1999). At 20 ka, the simulated ice area is $4.1 \times 10^4 \text{ km}^2$ which is nearly identical to the PATICE areal extent across our model domain (Figure 10). The ice margin at the Seno de Reloncaví, Lago Llanquihue, and other locations along the eastern boundary in the CLD advances slightly at 20 ka, but still remain inboard of the PATICE

Formatted: Font color: Text 1

Formatted: Font color: Text 1

Deleted: S

Deleted: and the main simulation.

Deleted:

Deleted: The difference in the simulated deglaciation age between sensitivity experiment

Deleted: and the main simulation

Formatted: Font color: Text 1

Deleted: .

Deleted: The difference in the simulated deglaciation age between sensitivity experiment 4 and the main simulation.

Formatted: Font color: Text 1

Commented [SMS]: There was a lot of redundant text here so I tried to reduce this a bit.

Formatted: Space After: Auto

Deleted: In Figure 8B the difference in the deglaciation age between sensitivity experiment 2 and the main simulation is shown, where precipitation is held constant at the monthly mean 12.5 ka- 12 ka value. Winter precipitation during this period is reduced modestly by up to 7% relative to the preindustrial across the model domain (Figure 7). Ice retreats faster across most of the CLD, along the ice margins and through the interior. Deglaciation along the margins occurs >1 kyr faster in many locations, and between 200 yrs to 1 kyr faster across portions of the ice interior.

In Figure 8C the difference in the deglaciation age between sensitivity experiment 3 and the main simulation is shown, where precipitation is held constant at the monthly mean 22 ka- 20 ka value. Winter precipitation during this period is increased by up to 10% relative to the preindustrial (Figure 7) across the northern portion of the model domain (north of 40°S), but is similar to preindustrial values across the southern portion of our model domain (south of 40°S). With the imposed higher precipitation across the northern portion of the model domain, ice retreats slower during the last deglaciation relative to our standard simulation by >1 kyr, and in some locations up to 2 kyr.

Deleted: <object><object>

Formatted: Font: Not Bold, Not Italic, Font color: Custom Color(RGB(31,127,198))

Deleted: The Trace-21ka model simulates upwards of 10-15% higher wintertime precipitation across the northern portion of our model domain during the LGM compared to preindustrial (Figure 3B, see TraCE-21ka). North of 40°S, wintertime precipitation is generally higher than the preindustrial until ~17.2 ka (Figure 9). Given the simulated increase in wintertime precipitation during the early deglacial (~22ka - 18ka; Figure 9) across the northern portion of the model domain, we run a sensitivity test to determine how thi [... [11]

Deleted:

Moved (insertion) [7]

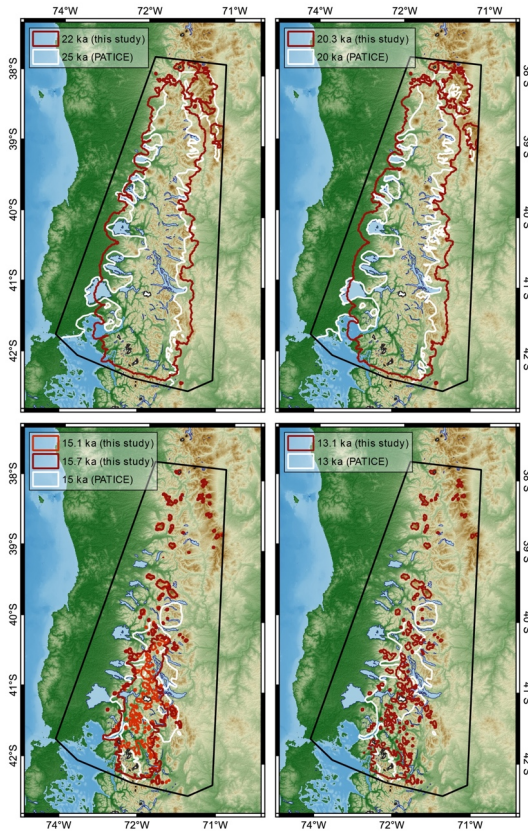


Figure 9. Comparison between the simulated ice extent at time intervals closest to the corresponding reconstructed ice extent from PATICE (Davies et al., 2020).

reconstruction for these regions. Between 18.3 ka and 15 ka large scale ice retreat occurs, and the simulated ice sheet loses 90% of its ice area, while the PATICE reconstruction suggests a reduction of 75% (Figure 10). At 15 ka, PATICE reconstructs an existing ice cap that separates from the remainder of the PIS to the south (Figure 9). This is in contrast to the simulated ice extent, which shows that by 15 ka, the PIS across our model domain has completely retreated and only mountain glaciers or small ice caps exist amongst the high terrain. However, if we compare the PATICE area at 15 ka and the simulated ice area at 15.7 ka (Figure 10), they are nearly identical at 1.2×10^4 km². While the PATICE ice extent at 15 ka and the simulated ice extent 15.7 ka do not match completely, the simulated ice extent at 15.7 ka still has evidence of a large ice cap similar to the PATICE reconstruction. Therefore, the simulated transition from ice sheet to ice cap and to discrete mountain glaciers occurs between 15.7 ka and 15 ka in our simulations. By 13 ka, our simulated ice area is 60% lower than the PATICE reconstructed area. By 10 ka this difference is

Deleted:

Deleted: 1410

Formatted: Font: Not Bold, Font color: Text 1, Pattern: Clear (White)

913 50%, however by this time the majority of the ice sheet has deglaciated (Figure 10), with our model
 914 simulating discrete mountain glaciers while PATICE reconstructs a small and narrow ice cap
 915 across the high terrain in the southern CLD (also see Figure 1).
 916
 917
 918

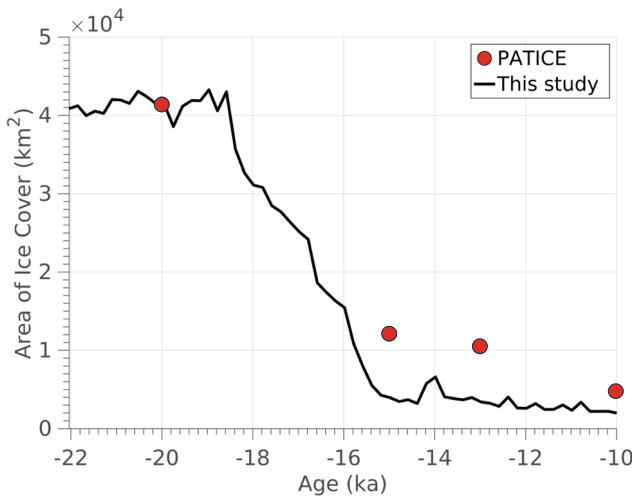


Figure 10. The simulated ice area (km²) from 22 ka to 10 ka shown as the black line. The red dots indicate the calculated ice area across our model domain for the reconstructed ice extent from PATICE (Davies et al., 2020).

919
 920 **4 Discussion**

921
 922 **4.1 Climate-ice sensitivity**

923 Determining the influence of the SWW on the heat and hydrologic budget across South America
 924 during the LGM and last deglaciation remains difficult, as limitations in paleo-proxy data and
 925 disagreement between climate models prohibit certainty (Kohfeld, 2013; Berman et al., 2018).
 926 And while evidence does suggest wetter conditions across the CLD during the late glacial (Moreno
 927 and Videla, 2018), linking the paleoclimate change in SWW position and strength from regional
 928 paleoclimate proxies remains problematic (Kohfeld et al., 2013).

929
 930 The scale at which we deduce ice history and climate interactions is also important. Looking at
 931 the PIS as a whole, recent numerical ice sheet modelling studies indicate that the simulated ice
 932 extent and volume for the entire PIS at the LGM is largely controlled by the magnitude of the
 933 temperature anomaly compared to present day (Yan et al., 2022). However, regional scale ice
 934 flow modelling informed by geologic constraints on past ice margin extent show that higher
 935 precipitation during the LGM (Leger et al., 2021), the late glacial, and the Holocene (Muir et al.,
 936 2023; Martin et al., 2022) is needed to support model-data agreement. It appears that during the
 937

Moved up [7]: Shown in Figure 1, PATICE assigns high to medium confidence to the reconstructed LGM (25 ka – 20 ka) ice extent along most of the western ice margin and portions of the eastern margin, with low confidence assigned to the northernmost ice extent. The majority of the ice history is poorly constrained (low confidence) during the deglaciation, and PATICE reconstructs a small cap that persists across the southern CLD until 10 ka, after which the ice disappears and only the Cerro Tronador glacier remains (see Figure 13 from Davies et al., 2020).

Deleted: ¶

Deleted:). ¶

Deleted: ¶

Deleted: We show the simulated and reconstructed ice extent in (Figure 910) as well as the calculated ice area from PATICE at 20 ka, 15 ka, 13 ka, and 103ka and for our transient simulation in (Figure 101). Overall, the 9 simulated ice margin and area is stable between 22 ka and 18.3 ka (Figure 11). At 22 ka (Figure 10), our model simulates a generally greater ice extent along the eastern and western margin, except at the Seno de Reloncavi, Golfo de Ancud, ~~object~~ and Lago Llanquihue, where the simulated ice margin does not advance to the well dated terminal LGM moraines (Mercer, 1972; Porter, 1981; Andersen et al., 1999; Denton et al., 1999). At 20 ka, the simulated ice area is 4.1x10⁴ km² which is nearly identical to the PATICE areal extent across our model domain (Figure 101). The ice margin at the Seno de Reloncavi, Lago Llanquihue, and other locations along the eastern boundary in the CLD advances slightly at 20 ka, but still remain inboard of the PATICE reconstruction for these regions. Between 18.3 ka and 15 ka large scale ice retreat occurs, and the simulated ice sheet loses 90% of its ice area, while the PATICE reconstruction suggests a reduction of 75% (Figure 1011). At 15 ka, PATICE reconstructs an existing ice cap that separates from the remainder of the PIS to the south (Figure 910). This is in contrast to the simulated ice extent, which shows that by 15 ka, the PIS across our model domain has completely retreated and only mountain glaciers or small ice caps exist amongst the high terrain. However, if we compare the PATICE area at 15 ka and the simulated ice area at 15.7 ka (Figure 101), they are nearly identical at 1.2x10⁴ km². While the PATICE ice extent at 15 ka and the simulated ice extent 15.7 ka do not match completely, the simulated ice extent at 15.7 ka still has evidence of a largen ice cap similar to the PATICE reconstruction. Therefore, the simulated transition from ice sheet to ice cap and to discrete mountain glaciers occurs between 15.7 ka and 15 ka in our simulations. By 13 ka, our simulated ice area is 60% (... [12])

Deleted: ~~object~~ ¶

Deleted: ¶

Deleted: elusive

Deleted: 6

Commented [CJK(3A6)]: In fact Kohfield does extensive analysis of paleo proxies to suggest that changes in hydrologic cycle do not necessarily have to be linked to changes in SWW, and is only 1 possible explanation (... [13])

1032 LGM a northward shift in the SWW (Kohfeld et al., 2013; Rojas et al., 2009; Togweillier et al.,
1033 2006) or a strengthening or expansion of the wind belt (Lamy et al., 2010) is perhaps the most
1034 likely scenario, with high frequency variability possible during the deglaciation as atmospheric
1035 reorganization altered the heat and hydrologic budget as recorded by glacier and ice sheet change
1036 (Davies et al., 2020; Boex et al., 2013).

1037
1038 We analyzed outputs of the wintertime (JJA) 925 hPa zonal wind as the mean over 500 yr periods
1039 from TraCE-21ka for the LGM (22-21ka), 18ka (18.5-18ka), 16ka (16.5-16ka), 14ka (14.5-14ka),
1040 12ka (12.5-12ka) and the Preindustrial (Supplemental section 3, Figures S3 A-E). Across our
1041 model domain and to its south, relative to the PI, zonal winds are stronger during the LGM with a
1042 southerly displacement (Figure S3A first and second column). During 18ka (Figure S3B), the zonal
1043 wind increases in strength relative to the PI, with the stronger winds having wider latitudinal
1044 coverage, particularly across our model domain. While the zonal mean position of the SWW is
1045 poleward at 18ka relative to the PI (Jiang and Yan, 2022), across Patagonia the simulated position
1046 of the maximum zonal wind is at the same latitudinal band as the PI. At 16ka, the zonal wind is
1047 stronger across our domain and Patagonia (Figure S3C) relative to the PI, although not as large as
1048 the differences during 18ka. By 14ka, the strength in the zonal winds across Patagonia and our
1049 model domain are similar to slightly stronger than the PI (Figure S3D), however, the zonal wind
1050 maximum is situated more equatorward across our model domain relative to the PI. By 12ka
1051 (Figure S3E), the zonal wind is similar to slightly weaker than the PI across our model domain,
1052 although it is stronger relative to the PI to the south of our model domain across central and
1053 southern Patagonia. The position of the maximum zonal winds is also displaced further south
1054 relative to the PI. These changes in strength and position of the simulated SWW during the last
1055 deglaciation are similar to the findings of Jian and Yan (2020), which found that relative to the
1056 Preindustrial (PI), TraCE-21ka simulates a more poleward subtropical and subpolar jet over the
1057 Southern hemisphere at the LGM. During the remainder of the LGM and last deglaciation, the
1058 overall position of the SWW migrates northward in TraCE-21ka, with poleward displacements
1059 during Heinrich Stadial 1 (HS1), equatorward displacements during the Antarctic Cold Reversal
1060 (ACR), and poleward displacements during the Younger Dryas (YD), similar to our analysis.

1061
1062 Additionally, we evaluated the wintertime (JJA) low-level (850 hPa) moisture flux convergence
1063 from TraCE-21ka (MFC; Supplement section 4, Figure S4A-E), which is influenced by the mean
1064 flow and transient eddies in the extratropical hydrologic cycle (Peixoto and Oort, 1992). During
1065 the LGM and 18 ka, MFC increases across our model domain, consistent with a convergence of
1066 the mean flow moisture fields relative to the PI (Figure S4 A, B). During the LGM and 18ka, we
1067 note that TraCE-21ka simulates higher JJA precipitation anomalies (relative to the PI) across our
1068 model domain (Figure 7). While our analysis cannot directly constrain the source of the positive
1069 precipitation anomalies (e.g., mean flow, storms), the strength of the simulated SWW in TraCE-
1070 21ka increases across our model domain (Figure S3 A, B) coincident with the increases in MFC,
1071 which may contribute to the positive precipitation anomalies at these time intervals (Figure 7). By
1072 16ka, there is increased divergence in the 925 hPa winds and moisture relative to the PI (Figure
1073 S4 C). Decreased MFC relative to the PI coincides with a reduction in precipitation across our
1074 model domain that is similar to or less than the PI (Figure 7). We note that the ice thickness
1075 boundary conditions used in the TraCE-21ka come from the Ice5G reconstruction (Peltier, 2004),
1076 which has the PIS being completely deglaciated by 16ka. However, our analysis cannot
1077 decompose whether the simulated changes in precipitation and MFC are a consequence of the

Formatted: Font color: Text 1

Deleted:

Deleted: . They evaluated the change in the SWW during the last 21,000 years using TraCE-21ka and

Deleted: find

Deleted: what

Deleted: finds

Formatted: Font: Not Italic, Font color: Text 1

Formatted: Font color: Text 1

Formatted: Font color: Text 1

Formatted: Font color: Text 1

1084 coupling between regional atmospheric circulation and the ice thickness boundary conditions used
1085 in TraCE-21ka or if these changes represent wider interactions with changes in hemispheric
1086 atmospheric circulation. By 14ka, and during the ACR, MFC increases relative to the PI (Figure
1087 S4D). This is consistent with a simulated equatorward migration of the SWW as shown in Jiang
1088 and Yan (2020) and our analysis (Figure S3D), and positive anomalies in precipitation across our
1089 model domain relative to the PI (Figure 7). By 12ka, precipitation across our model domain is
1090 reduced relative to the PI (Figure 7), and TraCE-21ka simulates a reduction in the MFC as well as
1091 a poleward migration of the SWW (Figure S3E; Jiang and Yan, 2020).

1093 When considering proxy records of precipitation across the CLD, there is reasonable agreement
1094 with the changes in precipitation simulated by TraCE-21ka. Moreno et al. (1999;2015) and
1095 Moreno and Videla (2018) find that wetter than present day conditions existed across the CLD
1096 during the LGM and early deglaciation which is consistent with the precipitation anomalies
1097 simulated by TraCE-21ka (Figure 7). These changes in paleoclimate proxies are attributed to an
1098 intensified storm track associated with an equatorward shift of the SWW (Moreno et al. 1999;
1099 2015). While TraCE-21ka instead simulates a poleward shift of the SWW during these time
1100 intervals, increases in precipitation and the intensification of the storm track as inferred by Moreno
1101 et al. (2015) may also be consistent with a strengthening of the SWW as simulated by TraCE-21ka
1102 during these intervals (Figure S3 A,B; Rojas et al., 2009; Sime et al., 2013; Kohfeld et al., 2013).
1103 Moreno et al. (2015) note that rapid warming ensues across the CLD around 17,800 cal yr BP,
1104 which is similar to the timing of deglacial warming as simulated by TraCE-21ka around 18.5 ka
1105 (Figure 6 top panel). Coincident with this rapid temperature rise, Moreno et al. (2015) note a shift
1106 from hyper humid to humid conditions which aligns well with decreases in the simulated
1107 precipitation in TraCE-21ka across our model domain (Figure 7). Lastly, Moreno et al. (1999;
1108 2015) find that colder and wetter conditions occur across the CLD during the ACR, and infer an
1109 equatorward expansion of the SWW as a potential cause. While TraCE-21ka simulates an abrupt
1110 and short ACR, it does simulate an equatorward expansion of the SWW (Figure S4 D; Jian and
1111 Yan, 2020), associated cooling (Figure 6 top panel), and increases in precipitation (Figure 7) that
1112 agree with the proxy data.

1114 Prior numerical ice flow modelling has indicated that precipitation played an important role in
1115 controlling the extent of paleoglaciers across the PIS (Muir et al., 2023; Leger et al., 2021) by
1116 modulating the pace and magnitude of ice retreat and advance during deglaciation (Martin et al.,
1117 2022). Much of the TraCE-21ka simulated winter precipitation anomalies shown in Figure 7 are
1118 within 10% of the preindustrial value. The sensitivity tests conducted here suggest that modest
1119 changes (~10%) in precipitation can alter the pace of ice retreat across the CLD on timescales
1120 consistent with the resolution of geochronological proxies constraining past ice retreat. We note
1121 that while TraCE-21ka simulates variations in precipitation across our model domain that are
1122 consistent with hydroclimate proxies discussed above (Moreno et al., 1999; 2015; 2018), the
1123 magnitude of those changes is not as large as proxy data across the CLD indicate. For example,
1124 hydroclimate proxies suggest that the LGM and early deglaciation was up to 2 times wetter across
1125 the CLD than present day (Moreno et al., 1999; Heusser et al., 1999). Therefore, we can deduce,
1126 from our sensitivity analysis here that higher precipitation anomalies during the LGM and last
1127 deglaciation, forced by proposed changes in the SWW (Moreno et al., 1999; 2015), may have
1128 helped offset melt from deglacial warming thereby influencing the pacing of early deglacial ice
1129 retreat in this region.

Deleted: ¶

Although our experimental setup cannot identify a clear relationship between the influence of temperature and precipitation on the simulated ice volume, these results indicate that the relationship is not simple. While the LGM cooling largely controls ice volume, wintertime precipitation, which comprises the majority of annual snow accumulation, can enhance or dampen the ice volume response to LGM temperature depressions (Figure 6). Using a small sample of LGM PMIP4 climate model output, we arrive at different simulated LGM states for the PIS across the CLD. If temperature were the primary control on ice volume, we would expect simulations using the coldest LGM climate model output to produce the highest LGM ice volumes (Figure 6). However, there are situations where this is not the case, as those simulations with higher precipitation produce higher ice volume despite modest LGM temperature depressions (i.e., Figure 6; IPSL). We note that the climate models with the coldest simulated LGM climate (AWI and MPI, Figure 3), correspondingly simulate the driest wintertime climate. Likewise models with higher spatial resolution, simulate a higher gradient in the simulated temperature and precipitation patterns. With discrepancy amongst climate model output, and a lack of paleo proxy data to constrain those models, these results illustrate that the relationship between LGM ice volume and extent across the CLD to climate is not simple as already suggested through prior work (Leger et al., 2021; Martin et al., 2022; Yan et al., 2022).

Deleted: ¶

¶

Deleted: critical

Deleted: of the

Deleted: and

Deleted: can

Deleted: e

Deleted: /

Deleted: past intervals

Deleted: Our sensitivity test (section 3.2.2) indicates that increases (~10%) in wintertime precipitation relative to preindustrial can offset ice loss driven by deglacial warming. In our case (Figure 7A, B), deglaciation is delayed across the northern portion of the model domain upwards of 1-2 kyr. Therefore, these results show that even modest changes in wintertime precipitation can modulate the pacing and magnitude of ice retreat driven by deglacial warming on scales that are recorded in the geologic record of ice margin migration, which has large implications for model-data comparisons seeking to evaluate the impact of deglacial climate change on past ice margin migration in this region.

Deleted: are

Deleted: t

1182
1183
1184
1185
1186
1187
1188
1189
1190
1191
1192
1193
1194
1195
1196
1197
1198
1199
1200
1201
1202
1203
1204
1205
1206
1207
1208
1209
1210
1211
1212
1213
1214
1215
1216
1217
1218
1219
1220
1221
1222
1223
1224
1225
1226
1227

4.2 Ice retreat *during* the Last Deglaciation

The PATICE dataset (Davies et al., 2020) serves as the best available reconstruction of ice margin change for the PIS across the last deglaciation. This state-of-the-art compilation provides an empirical reconstruction of the configuration of the PIS as isochrones every 5 ka, from 35 ka to present, based on detailed geomorphological data and available geochronological evidence. Because geochronological constraints on past PIS change are limited, the PATICE reconstruction assigns qualitative confidence to its reconstructed ice margins. Where there is agreement between geochronological and geomorphological indicators of past ice margin history (i.e., moraines), high confidence is assigned. Where geomorphological evidence suggests the existence of past ice margins, but lacks a geochronological constraint, medium confidence is assigned. Lastly, low confidence is assigned where there is a lack of any indicators of past ice sheet extent, where the ice limits result in interpolated interpretations from immediately adjacent moraines from valleys that have been mapped and dated. Across the CLD, the LGM ice extent is well constrained by geologic proxies particularly in the west and southwest (Figure 1). The moraines that constrain the piedmont ice lobes that formed along the western boundary are now presently lakes and have reasonable age control (Denton et al., 1999; Moreno et al., 1999; Lowell et al., 1995), giving confidence to the LGM ice margin limits. Beyond this region, age control is sparse along the western boundary for the timing of LGM ice extent, but the existence of well-defined moraines along lakes in the northern CLD are assumed to be in sync with those moraines deposited to the south (Denton et al., 1999). However, low confidence remains in the geologic reconstruction of the LGM ice boundary along the eastern margin where little to no chronological constraints are available. In general, deglaciation from the maximum LGM ice extent begins between 18 – 19 ka (Davies et al., 2020), however, poor age control and a lack of geomorphic indicators make it difficult to constrain the ice extent across this region during the deglaciation. For instance, a single cosmogenic nuclide surface exposure date retrieved from the Nahuel Huapi moraine yielded an age of ~31.4 ka (Zech et al., 2017). While it is assumed that the ice limit behaved similarly both to the west and east, the limited existing data prevents a comprehensive understanding of the ice extent at the northeastern margin. This induces the highest level of uncertainty in the reconstruction and hinders our data model comparison. Therefore, we rely on the PATICE dataset interpolated isochrones (low confidence) for this northeastern region as the state-of-the-art reconstruction.

In regards to ice area and extent, our simulated ice sheet at the LGM using TraCE-21ka climate boundary conditions agrees well with the PATICE reconstruction (Figure 10). Our simulations reveal that deglaciation began between 19 ka to 18 ka, consistent with the geologic proxies (Davies et al., 2020). The simulated ice retreat continues until 15 ka, with the largest pulses in ice mass loss occurring at 18.6 ka, 16.8 ka, and 16 ka (Figure 9). Where PATICE estimates an ice cap around 15 ka (~40°S), our simulations reveal that glaciation was restricted to high elevations. After 15 ka, mountain glaciers remain in our simulation but there is no presence of a large ice cap as reconstructed in PATICE. Comparison between the model simulations and PATICE becomes difficult during the 15 -13 ka period as confidence in the geologic reconstruction is low. Therefore, our model results offer a different reconstruction to PATICE, and indicate that the ice sheet in this region largely retreated by 15 ka, with only mountain glaciers remaining. However, during this interval, the Antarctic Cold Reversal (ACR) may have influenced the heat and hydrologic budget across this region, with wetter and cooler conditions interrupting the deglacial warming (Moreno

Deleted: across

Deleted: (i.e., moraines)

Formatted: Font color: Text 1

Deleted: The PATICE dataset (Davies et al., 2020) serves as the best available reconstruction of ice margin change for the PIS across the last deglaciation. Because geochronological constraints on past PIS change are limited, the PATICE reconstruction assigns qualitative confidence to its reconstructed ice margins. Where there is agreement between geochronological and geomorphological (i.e., moraines) indicators of past ice margin history, high confidence is assigned. Where geomorphological evidence suggests the existence of past ice margins, but lacks a geochronological constraint, medium confidence is assigned. Lastly, low confidence is assigned where there is a lack of any indicators of past ice sheet extent. Across the CLD, the LGM ice extent is well constrained by geologic proxies particularly in the west and southwest (Figure 1). The moraines that constrain the piedmont ice lobes that formed along the western boundary and are now presently lakes have reasonable age control (Denton et al., 1999; Moreno et al., 1999; Lowell et al., 1995) and give confidence to the LGM ice margin limits. Beyond this region, age control is sparse along the western boundary for the timing of LGM ice extent, but the existence of well-defined moraines along lakes in the northern CLD are assumed to be in sync with those moraines deposited to the south (Denton et al., 1999). Low confidence remains in the geologic reconstruction of the LGM ice boundary along the eastern margin. In general, deglaciation from the maximum LGM ice extent begins between 18 – 19 ka (Davies et al., 2020), however, poor age control and lack of geomorphic indicators make it difficult to constrain the ice extent across this region during the deglaciation.

Deleted: 11

Formatted: Font color: Text 1

Formatted: Font color: Text 1

1262 et al., 2018). While TraCE-21ka simulates a cooler and wetter ACR, it is short-lived, lasting about
1263 500 years as compared to 2,000 years in some ice core records or proxy-based studies (Lowry et
1264 al., 2019; He et al., 2013, Pedro et al., 2015). This potential for a favorable and prolonged period
1265 of glacier growth is likely missing in our simulations during the ACR, which may explain some of
1266 the mismatch against the PATICE reconstruction at 15 ka – 13 ka.

Deleted: n

Deleted:

Commented [MR7]: This is interesting because highlights the centennial-scale mass balance changes influenced and modulated by the SWW as suggested in the literature

Formatted: Font color: Text 1

1267 *4.3 Limitations*

1268 Currently ISSM is undergoing model developments to include a full treatment of solid earth-ice
1269 and sea-level feedbacks (Adhikari et al., 2016). Therefore, at this time, there is no coupling
1270 between the ice sheet and solid earth. Instead, we prescribed GIA from a global GIA model of the
1271 last glacial cycle from Caron et al. (2018). While this model reasonably estimates GIA across the
1272 PIS over the last deglaciation, our simulated ice history does not feedback onto GIA. The ice
1273 history for Patagonia incorporated into the Caron et al. (2018) ensemble is from Ivins et al. 2011.
1274 Therefore, the prescribed GIA response across our domain does not perfectly match our simulated
1275 ice history. Additionally, the global mantle from Caron et al. (2018) does not exhibit regional low
1276 viscosity that is attributable to Patagonia and therefore, current rates of deformation are likely
1277 underestimated by the model. By not simulating the 2-way coupled ice and solid-earth
1278 interactions, we could be missing some feedbacks between our simulated ice history and the solid
1279 earth that may modulate the deglaciation across this region. Despite this limitation however, our
1280 prescribed GIA from Caron et al. (2018) is reasonable when compared with reconstructed deglacial
1281 GIA in Patagonia (Troch et al., 2022), giving confidence that our simulation is capturing the
1282 regional influence of GIA on the simulated ice history.

Deleted: are

1283 Across most of our domain, there is evidence for an advance of piedmont glaciers across glacial
1284 outwash during the LGM, which formed the physical boundary for some of the existing terminal
1285 moraines around the lakes within the CLD (Bentley, 1996; Bentley, 1997). The formation of ice-
1286 contact proglacial lakes likely occurred as a function of deglacial warming and ice retreat (Bentley,
1287 1996). Where there were proglacial lakes along the westward ice front in the CLD, evidence
1288 suggests that ice was grounded during the LGM (Lago Puyehue; Heirman et al., 2011). During
1289 deglaciation, iceberg calving into the proglacial lakes may have occurred (Bentley 1996,1997;
1290 Davies et al., 2020), with evidence suggesting that local topography and calving may have
1291 controlled the spatially irregular timing of abandonment from the terminal moraines surrounding
1292 the proglacial lakes (Bentley, 1997). Recent glacier modelling (Sutherland et al., 2020) suggests
1293 that inclusion of ice-lake interactions may have large impacts on the magnitude and rate of
1294 simulated ice front retreat, as ice-lake interactions promote greater ice velocities, ice flux to the
1295 grounding line, and surface lowering. However, across our region Heirman et al. (2011) indicate
1296 that it is not well constrained how the proglacial lakes in the CLD may have influenced local
1297 deglaciation, and more geomorphic data is needed. Therefore, because the inclusion of ice-lake
1298 interactions is relatively novel for numerical ice flow modeling (Sutherland et al., 2020; Quiquet
1299 et al., 2021; Hinck et al., 2022), we choose to not simulate the evolution and influence of proglacial
1300 lakes on the deglaciation across this model domain. Given this limitation, our simulated magnitude
1301 and rate of ice retreat at the onset of deglaciation may be underestimated, especially when looking
1302 at local deglaciation along these proglacial lakes. Although we do not think that these processes
1303 would greatly influence our conclusions regarding the role of climate on the evolution of the PIS

Moved (insertion) [1]

Formatted: Font color: Text 1

Deleted: (

Formatted: Font color: Text 1

Deleted: The proglacial lake formation was likely coincident with However, because inclusion of ice-lake interactions is relatively novel for numerical ice flow modeling (Sutherland et al., 2020; Quiquet et al., 2021; Hinck et al., 2022), we choose to not model the evolution and influence of proglacial lakes on the deglaciation across this model domain.

Formatted: Font: (Default) Times New Roman, 12 pt, Font color: Text 1

Formatted: Font color: Text 1

Formatted: Font: (Default) Times New Roman, 12 pt, Font color: Text 1

Formatted: Font color: Text 1

Deleted: model

1318 is the CLD and the simulated ice retreat history, future work is required to assess the influence of
1319 proglacial lakes in this region.

1321 5 Conclusions

1322
1323 In this study, we use a numerical ice sheet model to simulate the LGM and deglacial ice history
1324 across the northernmost extent of the PIS, the CLD. The ice sheet model used inputs of
1325 temperature and precipitation from the TraCE-21ka climate model simulation covering the last
1326 22,000 years in order to simulate the deglaciation of the PIS across the CLD into the early
1327 Holocene.

1328
1329 Our numerical simulation suggests that large scale ice retreat occurs after 19 ka coincident with
1330 rapid deglacial warming, with the northern portion of the CLD becoming ice free by 17 ka. The
1331 simulated ice retreat agrees well with the most comprehensive geologic assessment of past PIS
1332 history available (PATICE; Davies et al., 2020) for the LGM ice extent and early deglacial but
1333 diverge when considering the ice geometry at and after 15 ka. In our simulations, the PIS persists
1334 until 15 ka across the remainder of the CLD, followed by ice retreat to higher elevations as
1335 mountain glaciers and small ice caps persist into the early Holocene (e.g., Cerro Tronador). The
1336 geologic reconstruction from PATICE instead estimates a small ice cap persisting across the
1337 southern portion of high terrain in the CLD until about 10 ka. However, of the limited geologic
1338 constraints particularly after 15 ka, high uncertainty in the timing and extent of deglacial ice history
1339 remains in the geologic reconstruction. Therefore, our results provide an additional reconstruction
1340 of the deglaciation of the PIS across the CLD that differs from PATICE after 15 ka, emphasizing
1341 a need for future work that aims to improve geologic reconstructions of past ice margin migration
1342 particularly during the later deglaciation across this region.

1343
1344 While deglacial warming was a primary driver of the demise of the PIS across the last deglaciation,
1345 we find that precipitation modulates the pacing and magnitude of deglacial ice retreat across the
1346 CLD. Paleoclimate proxies within the CLD has shown that the strength and position of the SWW
1347 varied during the LGM and last deglaciation, altering hydrologic patterns and influencing the
1348 deglacial mass balance. We find that the simulated changes in the strength and position of the
1349 SWW in TraCE-21ka are similar to those inferred from paleoclimate proxies of precipitation,
1350 consistent with a wetter than preindustrial climate being simulated and reconstructed over the CLD
1351 and in particular the region north of 40°S. Through a series of sensitivity tests, we alter the
1352 magnitude of the precipitation anomaly modestly (up to 10%) during our transient deglacial
1353 simulations and find that the pacing of ice retreat can speed up or slow down by a few hundred
1354 years and up to 2000 years depending on whether we impose an increase or decrease in the
1355 precipitation anomaly. While paleoclimate proxies of precipitation suggest that the CLD may have
1356 experienced twice as much precipitation during the LGM and early deglacial relative to present
1357 day (Moreno et al., 1999; 2015), TraCE-21ka simulates smaller increases in LGM and early
1358 deglacial precipitation (~10-15% greater than preindustrial). Therefore, while our modelling
1359 suggests that modest changes in precipitation can modulate the pace of deglacial ice retreat across
1360 the CLD, from our analysis we can deduct that larger anomalies in precipitation as found in the
1361 paleoclimate proxies may have an even larger impact on modulating deglacial ice retreat. Because
1362 paleoclimate proxies of past precipitation are often lacking, and climate models can simulate a
1363 range of possible LGM and deglacial hydrologic states, these results suggest that improved

Deleted: region

Deleted: Instead, we only simulate calving where the PIS interacts with the ocean.

Deleted: ¶

Deleted: relied

Deleted: on

Formatted: Font color: Text 1

Deleted: by

Formatted: Font color: Text 1

Formatted: Font color: Text 1

Deleted:

1372 [knowledge of the past precipitation is critical towards better understanding the drivers of PIS](#)
1373 [growth and demise, especially as small variations in precipitation can modulate ice sheet history](#)
1374 [on scales consistent with geologic proxies.](#)

1375 **Code/Data Availability**

1376 The simulations performed for this paper made use of the open-source Ice-Sheet and Sea-level
1377 System Model (ISSM) and are publicly available at <https://issm.jpl.nasa.gov/> (Larour et al., 2012).

1378 **Author Contribution**

1380 [JC and SM secured funding for this research. JC, MR, and SM all contributed to the project design.](#)
1381 [JC performed the model setup and simulations. JC performed the analyses on model output, with](#)
1382 [help from MR who performed analysis on PATICE reconstructions. JC wrote the manuscript with](#)
1383 [input from MR and SM.](#)

1384 **Competing interests**

1385 The contact author has declared that none of the authors has any competing interests.

1386 **Acknowledgements**

1387 This work was supported by a grant from the National Science Foundation, Frontier Research in
1388 Earth Sciences # 2121561.

1389 **References**

- 1390 Adhikari, S., Ivins, E. R., and Larour, E., 2016, ISSM-SESAW v1.0: mesh-based computation of
1391 gravitationally consistent sea level and geodetic signatures caused by cryosphere and
1392 climate driven mass change, *Geoscientific Model Development*, 9, 9769-9816, doi:
1393 10.5194/gmd-9-1087-2016.
- 1394 Åkesson, H., Morlighem, M., Nisancioglu, K. H., Svendsen, J. J., and Mangerud, J.:
1395 Atmosphere-driven ice sheet mass loss paced by topography: Insights from modelling the
1396 south-western Scandinavian Ice Sheet. 2018. *Quaternary Sci. Rev.*, 195, 32–
1397 47, <https://doi.org/10.1016/j.quascirev.2018.07.004>.
- 1398 Andersen, B., Denton, G. H., & Lowell, T. V. (1999). Glacial geomorphologic maps of
1399 Llanquihue drift in the area of the southern Lake District, Chile. *Geografiska Annaler:*
1400 *Series A, Physical Geography*, 81(2), 155-166.
- 1401 Bentley, M.J., 1996. The role of lakes in moraine formation, Chilean Lake District. *Earth*
1402 *Surf. Process. Landf.* 21, 493–507. [https://doi.org/10.1002/\(SICI\)1096-](https://doi.org/10.1002/(SICI)1096-9837(199606)21:6<493::AID-ESP612>3.0.CO;2-D)
1403 [9837\(199606\)21:6<493::AID-ESP612>3.0.CO;2-D](https://doi.org/10.1002/(SICI)1096-9837(199606)21:6<493::AID-ESP612>3.0.CO;2-D)
- 1404 Bentley, M.J., 1997. Relative and radiocarbon chronology of two former glaciers in the
1405 Chilean Lake District. *J. Quat. Sci.* 12, 25–33. [https://doi.org/10.1002/\(SICI\)1099-](https://doi.org/10.1002/(SICI)1099-1417(199701/02)12:1<25::AID-JQS289>3.0.CO;2-A)
1406 [1417\(199701/02\)12:1<25::AID-JQS289>3.0.CO;2-A](https://doi.org/10.1002/(SICI)1099-1417(199701/02)12:1<25::AID-JQS289>3.0.CO;2-A)
- 1407 Berman, L., Silvestri, G., Tonello, M.S., On differences between Last Glacial Maximum and
1408 Mid-Holocene climates in southern South America simulated by PMIP3 models. 2018.
1409 *Quat. Sci. Rev.* 185. 113-121. <https://doi.org/10.1016/j.quascirev.2018.02.003>.
- 1410 Blatter, H.: Velocity and stress-fields in grounded glaciers: A simple algorithm for including
1411 deviatoric stress gradients. 1995. *J. Glaciol.*, 41, 333-344,
1412 <https://doi.org/10.3189/S002214300001621X>

Deleted: ”

Deleted: In this study, we use a numerical ice sheet model to simulate the LGM and deglacial ice history across the northernmost extent of the PIS, the CLD. Our LGM ice sheet simulations were driven by climate model output from five climate models, providing a small ensemble of possible ice sheet states. Additionally, we used transient climate model output covering the last 21 kyr's to simulate the deglaciation of the PIS across the CLD into the early Holocene. ¶

¶ The position, strength, and extent of the SWW played an important role in modulating the size and response of the PIS deglaciation across the CLD. Our simulations indicate that during the LGM, the glacial cooling exerted a large control on the overall size of the PIS across the CLD. However, the simulated LGM precipitation, which varied considerably amongst the climate models, was shown to modulate the ice extent and ice volume across this region. This finding was corroborated by a transient simulation across the last deglaciation where the magnitude of simulated precipitation (in the TraCE-21ka climate model) was modestly higher during the LGM than the preindustrial across the northern portion of the CLD (~10% higher). These results suggest that increases in wintertime LGM and deglacial precipitation have the potential to modulate the timing and magnitude of ice retreat across the CLD. In our case, only modest increases in wintertime precipitation are needed to delay deglaciation up to 2 kyr in our sensitivity tests. Because paleoclimate proxies of past precipitation are often lacking, and climate models simulate a range of possible LGM and deglacial hydrologic states, these results suggest that knowledge of the past precipitation is critical towards better understanding the drivers of PIS growth and demise, especially as small variations in precipitation can modulate ice sheet history on scales consistent with geologic proxies. ¶

¶ Our transient simulation suggests that large scale deglaciation occurs after 19 ka, with the northern portion of the CLD becoming ice free by 17 ka. The PIS persists until 15 ka across the remainder of the CLD, before ice retreats to higher elevation as mountain glaciers and small ice caps (e.g. Cerro Tronador). These results generally agree with the most complete geologic assessment of past PIS history available (PATICE; Davies et al., 2020) for the LGM ice extent and early deglacial, but diverge when considering the ice geometry at and after 15 ka. Because of limited geologic constraints particularly after 15 ka, uncertainty in the timing and extent of deglacial ice history remains. Therefore, our results which illustrate the simulated PIS retreat across the CLD during the last deglaciation may provide insight for future work that aims to improve geologic reconstructions of past ice margin migration. ¶

Deleted: JC, MR, and SM all contributed to the project design. JC performed the model setup and simulations. JC performed the data analysis on model output, with help from MR who performed data analysis on PATICE reconstructions. JC wrote the manuscript with input from MR and SM. ¶

1476 Boex, J., Fogwill, C., Harrison, S. et al. Rapid thinning of the late Pleistocene Patagonian Ice
 1477 Sheet followed migration of the Southern Westerlies. 2013. *Sci Rep* **3**, 2118.
 1478 <https://doi.org/10.1038/srep02118>

1479 Boisier, J. P., Alvarez-Garretón, C., Cepeda, J., Osses, A., Vásquez, N., and Rondanelli, R.:
 1480 CR2MET: A high-resolution precipitation and temperature dataset for hydroclimatic
 1481 research in Chile. 2018. EGUGA, p. 19739.

1482 Braun, M.H., Malz, P., Sommer, C., Far.as-Barahona, D., Sauter, T., Casassa, G., Soruco,
 1483 A., Skvarca, P., Seehaus, T.C., 2019. Constraining glacier elevation and mass changes
 1484 in South America. *Nat. Clim. Chang.* **9**, 130–136. [https://doi.org/10.1038/s41558-018-](https://doi.org/10.1038/s41558-018-0375-7)
 1485 [0375-7](https://doi.org/10.1038/s41558-018-0375-7)

1486 [Brierley, C. M., Zhao, A., Harrison, S. P., Braconnot, P., Williams, C. J. R., Thornalley, D. J. R.,](https://doi.org/10.1038/s41558-018-0375-7)
 1487 [Shi, X., Peterschmitt, J.-Y., Ohgaito, R., Kaufman, D. S., Kageyama, M., Hargreaves, J.](https://doi.org/10.1038/s41558-018-0375-7)
 1488 [C., Erb, M. P., Emile-Geay, J., D'Agostino, R., Chandan, D., Carré, M., Bartlein, P. J.,](https://doi.org/10.1038/s41558-018-0375-7)
 1489 [Zheng, W., Zhang, Z., Zhuett, A. A., Csatho, B., de Vernal, A., Downs, J., Larour, E.,](https://doi.org/10.1038/s41558-018-0375-7)
 1490 [Peltier, W. R., Otto-Bliesner, B., Morozova, P. A., McKay, N. P., Lohmann, G., Legrande,](https://doi.org/10.1038/s41558-018-0375-7)
 1491 [A. N., Guo, C., Cao, J., Brady, E., Annan, J. D., and Abe-Ouchi, A.: Large-scale features](https://doi.org/10.1038/s41558-018-0375-7)
 1492 [and evaluation of the PMIP4-CMIP6 *midHolocene* simulations. *Clim. Past*, **16**, 1847–](https://doi.org/10.1038/s41558-018-0375-7)
 1493 [1872. <https://doi.org/10.5194/cp-16-1847-2020>. 2020.](https://doi.org/10.1038/s41558-018-0375-7)

1494 Briner, J. P., Cuzzone, J. K., Badgley, J. A., Young, N. E., Steig, E. J., Morlighem, M.,
 1495 Schlegel, N.-J., Hakim, G., Schaefer, J. Johnson, J. V., Lesnek, A. L., Thomas, E. K.,
 1496 Allan, E., Bennike, O., Cluett, A. A., Csatho, B., de Vernal, A., Downs, J., Larour, E.,
 1497 and Nowicki, S.: Rate of mass loss from the Greenland Ice Sheet will exceed Holocene
 1498 values this century. 2020. *Nature*, **6**, 70–74, <https://doi.org/10.1038/s41586-020-2742-6>.

1499 Bondzio, J. H., Seroussi, H., Morlighem, M., Kleiner, T., Rückamp, M., Humbert, A., and
 1500 Larour, E. Y.: Modelling calving front dynamics using a level-set method: application to
 1501 Jakobshavn Isbræ, West Greenland. 2016. *The Cryosphere*, **10**, 497–
 1502 510, <https://doi.org/10.5194/tc-10-497-2016>

1503 Budd, W.F., P. L. Keage, N. A. Blundy. Empirical studies of ice sliding. 1979. *J. Glaciol.*,
 1504 **23**:157-170.

1505 Caron, L., Ivins, E. R., Larour, E., Adhikari, S., Nilsson, J., and Blewitt, G.: GIA model statistics
 1506 for GRACE hydrology, cryosphere and ocean science. 2018. *Geophys. Res. Lett.*, **45**,
 1507 2203–2212, <https://doi.org/10.1002/2017GL076644>

1508 Choi, Y., Morlighem, M., Rignot, E., and Wood, M.: Ice dynamics will remain a primary driver
 1509 of Greenland ice sheet mass loss over the next century. 2021. *Commun. Earth Environ.*,
 1510 **2**, 26, <https://doi.org/10.1038/s43247-021-00092-z>

1511 [Clark, P.U., He, F., Golleddge, N.R., Mitrovica, J.X., Dutton, A., Hoffman, J.S., and Dendy, S.,](https://doi.org/10.1038/s41586-020-1931-7)
 1512 [2020, Oceanic forcing of penultimate deglacial and last interglacial sea-level rise: *Nature*,](https://doi.org/10.1038/s41586-020-1931-7)
 1513 [v. 577, p. 660–664, doi:10.1038/s41586-020-1931-7.](https://doi.org/10.1038/s41586-020-1931-7)

1514 Cuffey, K. M. and Paterson, W. S. B.: *The physics of glaciers*, 4th edn. 2010. Butterworth-
 1515 Heinemann, Oxford, ISBN 9780123694614

1516 Cuzzone, J. K., Schlegel, N.-J., Morlighem, M., Larour, E., Briner, J. P., Seroussi, H., and Caron,
 1517 L.: The impact of model resolution on the simulated Holocene retreat of the southwestern
 1518 Greenland ice sheet using the Ice Sheet System Model (ISSM). 2019. *The Cryosphere*,
 1519 **13**, 879–893, <https://doi.org/10.5194/tc-13-879-2019>.

1520 Cuzzone, J. K., Young, N. E., Morlighem, M., Briner, J. P., and Schlegel, N.-J.: Simulating the
 1521 Holocene deglaciation across a marine-terminating portion of southwestern Greenland in

Formatted: Default Paragraph Font, Font color: Text 1, Pattern: Clear

Formatted: Default Paragraph Font, Font color: Text 1, Pattern: Clear

Formatted: Font: (Default) Times New Roman, 12 pt, Font color: Text 1

Formatted: Justified, Indent: Hanging: 0.5"

Formatted: Indent: Hanging: 0.5", Line spacing: Multiple 1.1 li, No widow/orphan control, Adjust space between Latin and Asian text, Adjust space between Asian text and numbers, Border: Top: (No border), Bottom: (No border), Left: (No border), Right: (No border), Between : (No border)

Formatted: Pattern: Clear

1522 response to marine and atmospheric forcings. 2022. *The Cryosphere*, 16, 2355–2372,
1523 <https://doi.org/10.5194/tc-16-2355-2022>.

1524 Davies, B.J., Darvill, C.M., Lovell, H., Bendle, J.M., Dowdeswell, J.A., Fabel, D.,
1525 Gheorghiu, D.M., 2020. The evolution of the Patagonian ice sheet from 35 ka to
1526 the present day (PATICE). *Earth Sci. Rev.* 204, 103152. [https://doi.org/10.1016/](https://doi.org/10.1016/j.earscirev.2020.103152)
1527 [j.earscirev.2020.103152](https://doi.org/10.1016/j.earscirev.2020.103152).

1528 [Darvill, C.M., Stokes, C.R., Bentley, M.J., Evans, D.J.A., Lovell, H. 1996. Dynamics of former](#)
1529 [ice lobes of the southernmost Patagonian Ice Sheet based on glacial landsystems](#)
1530 [approach. *Journal of Quaternary Science*. 32, 6, 857-876.](#)
1531 <https://doi.org/10.1002/jqs.2890>

1532 [Darvill, C.M., Stokes, C.R., Bentley, M.J., Evans, D.J.A., Lovell, H., Dynamics of former ice](#)
1533 [lobes of the southernmost Patagonian Ice Sheet based on glacial landsystems approach.](#)
1534 [2017. *J. Quaternary Sci.*, 32:857-876. <https://doi.org/10.1002/jqs.2890>](#)

1535 [Denton, G.H., Lowell, T.V., Heusser, C.J., Schlüchter, C., Andersen, B.G., Heusser, L.E.,](#)
1536 [Moreno, P.I., Marchant, D.R., 1999. Geomorphology, Stratigraphy, and Radiocarbon](#)
1537 [Chronology of Llanquihue Drift in the Area of the Southern Lake District, Seno](#)
1538 [Reloncav., and Isla Grande de Chilo., Chile. *Geogr. Ann. Ser. A Phys. Geogr.* 81,](#)
1539 [167–229. <https://doi.org/10.1111/1468-0459.00057>](#)

1540 [Denton, G.H., Heusser, J., Lowell, T.V., Moreno, P.I., Andersen, B.G., Heusser, L.E., Schlüchter,](#)
1541 [C., Marchant, D.R. 1999. Interhemispheric Linkage of Paleoclimate During the Last](#)
1542 [Glaciation. *Geografiska Annaler*. 81, 2, 107-153. \[0459.00055\]\(https://doi.org/10.1111/1468-

1543 <a href=\)](#)

1544 Dias dos Santos, T., Morlighem, M., and Brinkerhoff, D.: A new vertically integrated Mono-
1545 Layer Higher-Order (MOLHO) ice flow model. 2022. *The Cryosphere*, 16, 179–195,
1546 <https://doi.org/10.5194/tc-16-179-2022>.

1547 [Díaz, C., Moreno, P. I., Villacís, L. A., Sepúlveda-Zúñiga, E. A., & Maidana, N. I. \(2023\).](#)
1548 [Freshwater diatom evidence for Southern Westerly Wind evolution since~ 18 ka in](#)
1549 [northwestern Patagonia. *Quaternary Science Reviews*. 316, 108231.](#)

1550 [Fernandez, A., Mark, B.G. 2016. Modeling modern glacier response to climate changes along the](#)
1551 [Andes Cordillera: A multiscale review, *J. Adv. Model. Earth Syst.*, 8, 467–495,](#)
1552 [doi:10.1002/2015MS000482.](#)

1553 Garreaud, R., Lopez, P., Minvielle, M., & Rojas, M. (2013). Large-scale control on the
1554 Patagonian climate. *Journal of Climate*, 26(1), 215-230.

1555 GEBCO Bathymetric Compilation Group 2021. 2021. The GEBCO_2021 Grid - a continuous
1556 terrain model of the global oceans and land. NERC EDS British Oceanographic Data
1557 Centre NOC. doi:10.5285/c6612cbe-50b3-0cff-e053-6c86abc09f8f

1558 Glasser, N. F., Jansson, K. N., Harrison, S., & Kleman, J. (2008). The glacial geomorphology
1559 and Pleistocene history of South America between 38 S and 56 S. *Quaternary Science*
1560 *Reviews*, 27(3-4), 365-390.

1561 Glen, J. W. The creep of polycrystalline ice. 1955. *P. Roy. Soc. Lond. A*, 228, 519–
1562 538, <https://doi.org/10.1098/rspa.1955.0066>.

1563 [Golledge, N. R., Thomas, Z. A., Levy, R. H., Gasson, E. G. W., Naish, T. R., McKay, R. M.,](#)
1564 [Kowalewski, D. E., and Fogwill, C. J.: Antarctic climate and ice-sheet configuration](#)
1565 [during the early Pliocene interglacial at 4.23 Ma, *Clim. Past*, 13, 959–975,](#)
1566 [Formatted: Default Paragraph Font, Font color: Text 1](https://doi.org/10.5194/cp-13-959-2017, 2017.</p>
</div>
<div data-bbox=)

Formatted: Indent: Left: 0", First line: 0.5"

Formatted: Default Paragraph Font, Font: (Default) Times New Roman, 12 pt, Font color: Text 1, Pattern: Clear

Formatted: Font: (Default) Times New Roman, 12 pt, Font color: Text 1

Formatted: Indent: Left: 0", Hanging: 0.5"

Formatted: Font: (Default) Times New Roman, 12 pt, Font color: Text 1

Formatted: Default Paragraph Font, Font: (Default) Times New Roman, 12 pt, Not Bold, Font color: Text 1

Formatted: Font:

Formatted

Formatted: Indent: Hanging: 0.5"

Formatted: English (US)

Formatted: Default Paragraph Font, Font color: Text 1

Formatted: Font: (Default) Times New Roman, 12 pt, Font color: Text 1

Formatted: Indent: Left: 0", Hanging: 0.5"

1567 Hajima, T., Watanabe, M., Yamamoto, A., Tatebe, H., Noguchi, M. A., Abe, M., Ohgaito, R.,
1568 Ito, A., Yamazaki, D., Okajima, H., Ito, A., Takata, K., Ogochi, K., Watanabe, S., and
1569 Kawamiya, M.: Development of the MIROC-ES2L Earth system model and the
1570 evaluation of biogeochemical processes and feedbacks, *Geosci. Model Dev.*, 13, 2197–
1571 2244, <https://doi.org/10.5194/gmd-13-2197-2020>

1572 He, F., Shakun, J. D., Clark, P. U., Carlson, A. E., Liu, Z., Otto-Bliesner, B. L., Kutzbach, J. E.
1573 2013. Northern Hemisphere forcing of Southern Hemisphere climate during the last
1574 deglaciation, *Nature*, 494, 81–85. doi: 10.1038/nature11822.

1575 [He, F., Clark, P.U. 2022. Freshwater forcing of the Atlantic Meridional Overturning Circulation](#)
1576 [revisited. *Nature Climate Change*. 12. 449-454. \[https://doi.org/10.1038/s41558-022-\]\(https://doi.org/10.1038/s41558-022-01328-2\)](#)
1577 [01328-2.](#)

1578 Heirman, K., De Batist, M., Charlet, F., Moernaut, J., Chapron, E., Brümmner, R., Pino, M.,
1579 Urrutia, R., 2011. Detailed seismic stratigraphy of Lago Puyehue: implications for the
1580 mode and timing of glacier retreat in the Chilean Lake District. *J. Quat. Sci.* 26,
1581 665–674. <https://doi.org/10.1002/jqs.1491>

1582 Hinck, S., Gowan, E. J., Zhang, X., and Lohmann, G.: PISM-LakeCC: Implementing an adaptive
1583 proglacial lake boundary in an ice sheet model. 2022. *The Cryosphere*, 16, 941–965,
1584 <https://doi.org/10.5194/tc-16-941-2022>.

1585 Hubbard, A., Hein, A.S., Kaplan, M.R., Hulton, N.R.J., Glasser, N., 2005. A modelling
1586 reconstruction of the last glacial maximum ice sheet and its deglaciation in the
1587 vicinity of the northern Patagonian icefield, south America. *Geogr. Ann. Phys.Geogr.* 87
1588 (2), 375-391. <https://doi.org/10.1111/j.0435-3676.2005.00264.x>

1589 Hulton, N.R.J., Purves, R., McCulloch, R., Sugden, D.E., Bentley, M.J., 2002. The last
1590 glacial maximum and deglaciation in southern south America. *Quat. Sci. Rev.* 21
1591 (1), 233-241. [https://doi.org/10.1016/S0277-3791\(01\)00103-2](https://doi.org/10.1016/S0277-3791(01)00103-2).

1592 Hulton, N., Sugden, D., Payne, A., Clapperton, C., 1994. Glacier modeling and the
1593 climate of Patagonia during the last glacial maximum. *Quat. Res.* 42 (1), 1-19.
1594 doi:10.1006/qres.1994.1049

1595 Jiang, N., Yan, Q. Evolution of the meridional shift of the subtropical and subpolar westerly jet
1596 over the Southern Hemisphere during the past 21,000 years. 2020. *Quat Sci. Rev.* 246,
1597 <https://doi.org/10.1016/j.quascirev.2020.106544>.

1598 Kilian, R., Lamy, F., 2012. A review of Glacial and Holocene paleoclimate records
1599 from southernmost Patagonia (49e55 S). *Quat. Sci. Rev.* 53,
1600 doi.10.1016/j.quascirev.2012.07.017

1601 [Kageyama, M., Harrison, S. P., Kapsch, M.-L., Lofverstrom, M., Lora, J. M., Mikolajewicz, U.,](#)
1602 [Sherriff-Tadano, S., Vadsaria, T., Abe-Ouchi, A., Bouttes, N., Chandan, D., Gregoire, L.](#)
1603 [J., Ivanovic, R. F., Izumi, K., LeGrande, A. N., Lhardy, F., Lohmann, G., Morozova, P.](#)
1604 [A., Ohgaito, R., Paul, A., Peltier, W. R., Poulsen, C. J., Quiquet, A., Roche, D. M., Shi,](#)
1605 [X., Tierney, J. E., Valdes, P. J., Volodin, E., and Zhu, J. 2021. The PMIP4 Last Glacial](#)
1606 [Maximum experiments: preliminary results and comparison with the PMIP3 simulations.](#)
1607 [*Clim. Past*, 17, 1065–1089, <https://doi.org/10.5194/cp-17-1065-2021>.](#)

1608 [Kilian, R., Lamy, F. A review of Glacial and Holocene paleoclimate records from southernmost](#)
1609 [Patagonia \(49-55°S\). 2012. 53, 15, 1-23.](#)
1610 [https://doi.org/10.1016/j.quascirev.2012.07.017](#)

1611 Kohfeld, K.E., Graham, R.M., Boer, A. M. de, Sime, L.C., Wolff, E.W., Qu er e, C.L.,
1612 Bopp, L., 2013. Southern Hemisphere westerly wind changes during the Last

Formatted: Indent: Hanging: 0.5"

Formatted: Font: (Default) Times New Roman, Font color: Text 1

Deleted: ¶

Formatted: Indent: First line: 0.5"

Deleted: Darvill, C.M., Stokes, C.R., Bentley, M.J., Evans, D.J.A., Lovell, H., Dynamics of former ice lobes of the southernmost Patagonian Ice Sheet based on glacial landsystems approach. 2017. *J. Quaternary Sci.*, 32:857-876. <https://doi.org/10.1002/jqs.2890>
Denton, G.H., Lowell, T.V., Heusser, C.J., Schlüchter, C., Andersen, B.G., Heusser, L.E.,
Moreno, P.I., Marchant, D.R., 1999. Geomorphology, Stratigraphy, and Radiocarbon Chronology of Llanquihue Drift in the Area of the Southern Lake District, Seno Reloncav., and Isla Grande de Chilo., Chile. *Geogr. Ann. Ser. A Phys. Geogr.* 81, 167–229.

Formatted: Font: (Default) Times New Roman, 12 pt, Font color: Text 1

Formatted: Font:

Formatted: Indent: Left: 0", Hanging: 0.56"

Formatted

Formatted: Font: (Default) Times New Roman, 12 pt, Font color: Text 1,

Formatted

1628 Glacial Maximum: paleo-data synthesis. *Quat. Sci. Rev.* 68, 76-95. ,
 1629 10.1016/j.quascirev.2013.01.017

1630 Lamy, F., Kilian, R., Arz, H.W., Francois, J.-P., Kaiser, J., Prange, M., Steinke, T., 2010.
 1631 Holocene changes in the position and intensity of the southern westerly wind belt. *Nat.*
 1632 *Geosci.* 3, 695–699. <https://doi.org/10.1038/ngeo959>

1633 Lamy, F., Arz, H. W., Kilian, R., Lange, C. B., Lembke-Jene, L., Wengler, M., ... & Tiedemann,
 1634 R. (2015). Glacial reduction and millennial-scale variations in Drake Passage
 1635 throughflow. *Proceedings of the National Academy of Sciences*, 112(44), 13496-13501
 1636 <https://doi.org/10.1073/pnas.1509203112>

1637 Larour, E., Seroussi, H., Morlighem, M., and Rignot, E.: Continental scale, high order, high
 1638 spatial resolution, ice sheet modeling using the Ice Sheet System Model (ISSM). 2012. *J.*
 1639 *Geophys. Res.-Earth*, 117, F01022, <https://doi.org/10.1029/2011JF002140>

1640 Le Morzadec, K., Tarasov, L., Morlighem, M., and Seroussi, H.: A new sub-grid surface mass
 1641 balance and flux model for continental-scale ice sheet modelling: testing and last glacial
 1642 cycle. 2015. *Geosci. Model Dev.*, 8, 3199–3213, [https://doi.org/10.5194/gmd-8-3199-](https://doi.org/10.5194/gmd-8-3199-2015)
 1643 2015

1644 Leger TPM, Hein AS, Goldberg D, Schimmelpfennig I, Van Wyk de Vries MS, Bingham RG and
 1645 ASTER Team (2021) Northeastern Patagonian Glacier Advances (43°S) Reflect
 1646 Northward Migration of the Southern Westerlies Towards the End of the Last Glaciation.
 1647 *Front. Earth Sci.* 9:751987. doi: 10.3389/feart.2021.751987

1648 Liu, Z., Otto-Bliesner, B., He, F., Brady, E., Tomas, R., Clark, P., Carlson, A., Lynch-Stieglitz,
 1649 J., Curry, W., Brook, E., Erickson, D., Jacob, R., Kutzbach, J., and Cheng, J. 2009.
 1650 Transient simulation of last deglaciation with a new mechanism for Bølling-Allerød
 1651 warming. *Science*, 325, 310–314. <https://doi.org/10.1126/science.1171041>

1652 Lowry, D. P., Golledge, N. R., Menviel, L., and Bertler, N. A. N.: Deglacial evolution of
 1653 regional Antarctic climate and Southern Ocean conditions in transient climate
 1654 simulations. 2019. *Clim. Past*, 15, 189–215, <https://doi.org/10.5194/cp-15-189-2019>.

1655 Lowell, T., Heusser, C., Andersen, B., Moreno, P., Hauser, A., Heusser, L., Schlüchter,
 1656 C., Marchant, D., Denton, G., 1995. Interhemispheric correlation of late Pleistocene glacial
 1657 events. *Science* 269, 1541–1549. Doi: 10.1126/science.269.5230.1541

1658 Lowry, D. P., Golledge, N. R., Menviel, L., and Bertler, N. A. N.: Deglacial evolution of
 1659 regional Antarctic climate and Southern Ocean conditions in transient climate
 1660 simulations. 2019. *Clim. Past*, 15, 189–215, <https://doi.org/10.5194/cp-15-189-2019>

1661 [Marcott, S.A., Shakun, J.D., Clark, P.U., Mix, A.C. 2013. A Reconstruction of Regional and](#)
 1662 [Global Temperature for the Past 11,300 Years. 339, 6124, 1198-1201. DOI:](#)
 1663 [10.1126/science.1228026](#)

1664 Martin J, Davies BJ, Jones R and Thorndycraft V (2022), Modelled sensitivity of Monte San
 1665 Lorenzo ice cap, Patagonian Andes, to past and present climate. *Front. Earth Sci.*
 1666 10:831631. doi: 10.3389/feart.2022.831631

1667 Mauritsen, T., Bader, J., Becker, T., Behrens, J., Bittner, M., Brokopf, R., Brovkin, V., Claussen,
 1668 M., Crueger, T., Esch, M., Fast, I., Fiedler, S., Fläschner, D., Gayler, V., Giorgetta, M.,
 1669 Goll, D. S., Haak, H., Hagemann, S., Hedemann, C., Hohenegger, C., Ilyina, T., Jahns, T.,
 1670 Jimenez-de-la-Cuesta, D., Jungclaus, J., Kleinen, T., Kloster, S., Kracher, D., Kinne, S.,
 1671 Kleberg, D., Lasslop, G., Kornbluh, L., Marotzke, J., Matei, D., Meraner, K.,
 1672 Mikolajewicz, U., Modali, K., Möbis, B., Müller, W. A., Nabel, J. E. M. S., Nam, C. C.

Formatted: Indent: Left: 0", Hanging: 0.56"

Moved down [6]: Pfeffer, W.T., Arendt, A.A., Bliss, A., Bolch, T., Cogley, J.G., Gardner, A.S., Hagen, J.O., Hock, R., Kaser, G., Kienholz, C. and Miles, E.S. 2014. The Randolph Glacier Inventory: a globally complete inventory of glaciers. *Journal of Glaciology*, 60, 537-552. Doi:10.3131/2014JoG13J176

Deleted:

Formatted: Default Paragraph Font, Font color: Text 1, Pattern: Clear

Formatted: Indent: Hanging: 0.5"

Formatted: Default Paragraph Font, Font: Times New Roman, 12 pt, Font color: Text 1, Pattern: Clear

1680 W., Notz, D., Nyawira, S.-S., Paulsen, H. Peters, K., Pincus, R., Pohlmann, H. Pongratz,
1681 J., Popp, M., Raddatz, T. J., Rast, S., Redler, R., Reick, C. H., Rohrschneider, T.,
1682 Schemann, V., Schmidt, H., Schnur, R., Schulzweida, U., Six, K. D., Stein, L., Stemmler,
1683 I., Stevens, B., von Storch, J.-S., Tian, F., Voigt, A., Vrese, P., Wieners, K.-H.,
1684 Wilkenskjeld, S., Winkler, A., and Roeckner, E.: Developments in the MPI-M Earth
1685 System Model version 1.2 (MPI-ESM1.2) and its response to increasing CO₂, J. Adv.
1686 Model. Earth Syst. 2019. 11, 998–1038, <https://doi.org/10.1029/2018MS001400>
1687 Meier, W.J-H., Griefßinger, J., Hochreuther, P., Braun, M.H. 2018. An updated multi-temporal
1688 glacier inventory for the Patagonian Andes with changes between the Little Ice Age and
1689 2016. *Frontiers in Earth Science*, 6, 62. <https://doi.org/10.3389/feart.2018.00062>
1690 Menviel, L., A. Timmermann, A. Mouchet, and O. Timm, 2008: Climate and marine carbon
1691 cycle response to changes in the strength of the Southern Hemispheric
1692 westerlies. *Paleoceanography*, 23, PA4201, doi:10.1029/2008PA001604.
1693 Mercer, J.H., 1972. Chilean glacial chronology 20,000 to 11,000 carbon-14 years ago:some
1694 global comparisons. *Science* 176, 1118–1120. DOI: 10.1126/science.176.4039.1118
1695 Moreno, P. I., Lowell, T. V., Jacobson Jr, G. L., & Denton, G. H. (1999). Abrupt vegetation and
1696 climate changes during the last glacial maximum and last termination in the Chilean lake
1697 district: a case study from Canal de la Puntilla (41°S). *Geografiska Annaler: Series A,*
1698 *Physical Geography*, 81(2), 285–311.
1699 Moreno, P.I., Denton, G.H., Moreno, H., Lowell, T.V., Putnam, A.E., Kaplan, M.R., 2015.
1700 Radiocarbon chronology of the last glacial maximum and its termination in
1701 northwestern Patagonia. *Quat. Sci. Rev.* 122, 233e249. 10.1016/j.quascirev.2015.05.027
1702 Moreno, P.I., Videla, J., Valero-Garcés, B.L., Alloway, B.V., Heusser, L.E., 2018.
1703 A continuous record of vegetation, fire-regime and climatic changes in northwestern
1704 Patagonia spanning the last 25,000 years. *Quat. Sci. Rev.* 198,
1705 10.1016/j.quascirev.2018.08.013
1706 Morlighem, M., Bondzio, J., Seroussi, H., Rignot, E., Larour, E., Humbert, A., and Rebuffi, S.:
1707 Modeling of Store Gletscher's calving dynamics, West Greenland, in response to ocean
1708 thermal forcing. 2016. *Geophys. Res. Lett.*, 43, 2659–
1709 2666, <https://doi.org/10.1002/2016GL067695>
1710 Muir, R., Eaves, S., Vargo, L., Anderson, B., Mackintosh, A., Sagredo, E., Soteres, R. Late
1711 glacial climate evolution in the Patagonian Andes (44–47°S) from alpine glacier modelling.
1712 2023. *Quaternary Science Reviews*, 305, <https://doi.org/10.1016/j.quascirev.2023.108035>.
1713 Ohgaito, R., Yamamoto, A., Hajima, T., O'ishi, R., Abe, M., Tatebe, H., Abe-Ouchi, A., and
1714 Kawamiya, M.: PMIP4 experiments using MIROC-ES2L Earth system model, *Geosci.*
1715 *Model Dev.*, 14, 1195–1217, <https://doi.org/10.5194/gmd-14-1195-2021>
1716 Pattyn, F.: A new three-dimensional higher-order thermomechanical ice sheet model:
1717 Basic sensitivity, ice stream development, and ice flow across subglacial lakes. 2003. *J.*
1718 *Geophys. Res.*, 108, 2382, <https://doi.org/10.1029/2002JB002329>
1719 Pedro, J. B., Bostock, H. C., Bitz, C. M., He, F., Vandergoes, M. J., Steig, E. J., Chase, B.M.,
1720 Krause, C.E., Rasmussen, S.O., Bradley, M.R., Cortese, G. 2016. The spatial extent and
1721 dynamics of the Antarctic Cold Reversal. *Nature Geoscience*, 9(1), 51–55.
1722 <https://doi.org/10.1038/ngeo2580>
1723 Peixoto, J. P., and A. H. Oort (1992), *Physics of Climate*, American Institute of Physics,
1724 520 pp.

Formatted: Emphasis, Font color: Text 1

Formatted: Font: 12 pt, Font color: Text 1

Formatted: Default Paragraph Font, Font color: Custom Color(RGB(34,34,34)), Pattern: Clear

Formatted: Font color: Text 1

Formatted: Indent: Left: 0", Hanging: 0.5"

1725 [Pfeffer, W.T., Arendt, A.A., Bliss, A., Bolch, T., Cogley, J.G., Gardner, A.S., Hagen, J.O., Hock,](#)
1726 [R., Kaser, G., Kienholz, C. and Miles, E.S. 2014. The Randolph Glacier Inventory: a](#)
1727 [globally complete inventory of glaciers. *Journal of Glaciology*, 60, 537-552.](#)
1728 [Doi:10.313189/2014JoG13J176](#)

1729 Pollard, D. and DeConto, R. M.: Description of a hybrid ice sheet-shelf model, and application to
1730 Antarctica. 2012. *Geosci. Model Dev.*, 5, 1273–1295, [https://doi.org/10.5194/gmd-5-](https://doi.org/10.5194/gmd-5-1273-2012)
1731 1273-2012.

1732 Porter, S. C. (1981). Pleistocene glaciation in the southern Lake District of Chile. *Quaternary*
1733 *Research*, 16(3), 263-292.

1734 Quiquet, A., Dumas, C., Paillard, D., Ramstein, G., Ritz, C., and Roche, D. M.: Deglacial Ice
1735 Sheet Instabilities Induced by Proglacial Lakes. 2021. *Geophys. Res. Lett.*, 48,
1736 e2020GL092141, <https://doi.org/10.1029/2020GL092141>

1737 Rojas, M., Moreno, P., Kageyama, M., Crucifix, M., Hewitt, C., Abe-Ouchi, A., Ohgaito, R.,
1738 Brady, E.C., Hop, P. 2009. The Southern Westerlies during the last glacial maximum in
1739 PMIP2 simulations. *Clim. Dyn.* 32, 525–548. [https://doi.org/10.1007/s00382-008-0421-](https://doi.org/10.1007/s00382-008-0421-7)
1740 [7.](#)

1741 [Rojas, M., 2013. Sensitivity of southern Hemisphere circulation to LGM and 4 CO2](#)
1742 [climates. *Geophys. Res. Lett.* 40, 965e970.](#)

1743 [Sepulchre, P., Caubel, A., Ladant, J.-B., Bopp, L., Boucher, O., Braconnot, P., Brockmann, P.,](#)
1744 [Cozic, A., Donnadiou, Y., Dufresne, J.-L., Estella-Perez, V., Ethé, C., Fluteau, F.,](#)
1745 [Foujols, M.-A., Gastineau, G., Ghattas, J., Hauglustaine, D., Hourdin, F., Kageyama, M.,](#)
1746 [Khadri, M., Marti, O., Meurdesoif, Y., Mignot, J., Sarr, A.-C., Servonnat, J.,](#)
1747 [Swingedouw, D., Szopa, S., and Tardif, D.: IPSL-CM5A2 – an Earth system model](#)
1748 [designed for multi-millennial climate simulations, *Geosci. Model Dev.*, 2020. 13, 3011–](#)
1749 [3053, <https://doi.org/10.5194/gmd-13-3011-2020>](#)

1750 [Seguinot, J., Rogozhina, I., Stroeven, A. P., Margold, M., and Kleman, J.: Numerical simulations](#)
1751 [of the Cordilleran ice sheet through the last glacial cycle, *The Cryosphere*, 10, 639–664,](#)
1752 [https://doi.org/10.5194/tc-10-639-2016, 2016.](#)

1753 [Shakun, J., Clark, P., He, Marcott, S.A., Mix, A. C., Liu, A., Otto-Bliesner, B., Schmittner, A.,](#)
1754 [Bards, E. 2012. Global warming preceded by increasing carbon dioxide concentrations](#)
1755 [during the last deglaciation. *Nature* 484, 49–54. <https://doi.org/10.1038/nature10915>](#)

1756 [Shakun, J.D., Lea, D.W., Lisiecki, L.E., Raymo, M.E. 2015. An 800-kyr record of global](#)
1757 [surface ocean δ18O and implications for ice volume-temperature coupling. 426, 58-68.](#)
1758 [https://doi.org/10.1016/j.epsl.2015.05.042](#)

1759 [Sidorenko, D., Goessling, H., Koldunov, N., Scholz, P., Danilov, S., Barbi, D., Cabos, W.,](#)
1760 [Gurses, O., Harig, S., Hinrichs, C., Juricke, S., Lohmann, G., Losch, M., Mu, L.,](#)
1761 [Rackow, T., Rakowsky, N., Sein, D., Semmler, T., Shi, X., Stepanek, C., Streffing, J.,](#)
1762 [Wang, Q., Wekerle, C., Yang, H., and Jung, T.: Evaluation of FESOM2.0 Coupled to](#)
1763 [ECHAM6.3: Preindustrial and High- ResMIP Simulations, 2019. *J. Adv. Model. Earth*](#)
1764 [Sy., 11, 3794–3815, <https://doi.org/10.1029/2019MS001696>](#)

1765 [Sime, L. C., K. E. Kohfeld, C. Le Quéré, E. W. Wolff, A. M. de Boer, R. M. Graham,](#)
1766 [and L. Bopp, 2013: Southern Hemisphere westerly wind changes during the Last Glacial](#)
1767 [Maximum: Model–data comparison. *Quat. Sci. Rev.*, 64, 104–](#)
1768 [120, <https://doi.org/10.1016/j.quascirev.2012.12.008>.](#)

1769 [Sugden, D. E., N. R. J. Hulton, and R. S. Purves \(2002\). Modelling the inception of the](#)
1770 [Patagonian icesheet, *Quat. Int.*, 95 – 96, 55 – 64. DOI:10.1016/S0277-3791\(01\)00103-2](#)

Moved (insertion) [6]

Formatted: Indent: Hanging: 0.5"

Formatted: Default Paragraph Font, Font color: Text 1, Pattern: Clear

Formatted: Font: 12 pt, Font color: Text 1

Formatted: Indent: Left: 0", First line: 0.5"

Moved down [5]: Tarasov, L. and Peltier, R. W.: Impact of thermomechanical ice sheet coupling on a model of the 100 kyr ice age cycle. 1999. *J. Geophys. Res.-Atmos.*, 104, 9517–9545

Tozer, B., Sandwell, D.T., Smith, W.H.F., Olsen, S.C., Beale, J.R., Wessel, P. Global Bathymetry and Topography at 15 Arc Sec: SRTM15+. 2019. *Earth and Space Science*. 6, 10, 1847-1864. <https://doi.org/10.1029/2019EA000658>

Deleted: Kageyama, M., Harrison, S. P., Kapsch, M.-L., Lofverstrom, M., Lora, J. M., Mikolajewicz, U., Sherriff-Tadano, S., Vadsaria, T., Abe-Ouchi, A., Bouttes, N., Chandan, D., Gregoire, L. J., Ivanovic, R. F., Izumi, K., LeGrande, A. N., Lhardy, F., Lohmann, G., Morozova, P. A., Ohgaito, R., Paul, A., Peltier, W. R., Poulsen, C. J., Quiquet, A., Roche, D. M., Shi, X., Tierney, J. E., Valdes, P. J., Volodin, E., and Zhu, J. 2021. The PMIP4 Last glacial maximum experiments: preliminary results and comparison with the PMIP3 simulations. *Clim. Past*, 17, 1065–1089, <https://doi.org/10.5194/cp-17-1065-2021>

Formatted: Default Paragraph Font, Font color: Text 1, Pattern: Clear

Formatted: Font: (Default) Times New Roman, 12 pt, Font color: Text 1

Formatted: Font: (Default) Times New Roman, Font color: Text 1

Formatted: Font: (Default) Times New Roman, Not Bold, Font color: Text 1

Formatted: Font: (Default) Times New Roman, Font color: Text 1

Formatted: Font color: Text 1

Formatted: Indent: Left: 0", Hanging: 0.5"

Formatted: Font: (Default) Times New Roman, Font color: Text 1

Deleted: ¶

Formatted: Default Paragraph Font, Font color: Text 1, Pattern: Clear

Formatted: Font: 12 pt, Font color: Text 1

Formatted: Font: 12 pt, No underline, Font color: Text 1

Formatted: Font: 12 pt, Font color: Text 1

Formatted: Font color: Text 1

Formatted: Font: Times New Roman, 12 pt, Font color: Text 1

Formatted: Default Paragraph Font, Font: Times New Roman, 12 pt, Font color: Text 1, Border: (No border), Pattern: Clear

1792 Sutherland, J. L., Carrivick, J. L., Gandy, N., Shulmeister, J., Quincey, D. J., and Cornford, S. L.:
 1793 Proglacial Lakes Control Glacier Geometry and Behavior During Recession. 2020.
 1794 Geophys. Res. Lett., 47, e2020GL088865, <https://doi.org/10.1029/2020GL088865>
 1795 Tarasov, L. and Peltier, R. W.: Impact of thermomechanical ice sheet coupling on a model of the
 1796 100 kyr ice age cycle. 1999. J. Geophys. Res.-Atmos., 104, 9517–9545
 1797 Tozer, B., Sandwell, D.T., Smith, W.H.F., Olsen, S.C., Beale, J.R., Wessel, P. Global
 1798 Bathymetry and Topography at 15 Arc Sec: SRTM15+. 2019. Earth and Space Science,
 1799 6, 10. 1847-1864. <https://doi.org/10.1029/2019EA000658>,
 1800 Tigchelaar, M., Timmermann, A., Friedrich, T., Heinemann, M., and Pollard, D.: Nonlinear
 1801 response of the Antarctic Ice Sheet to late Quaternary Sea level and climate forcing. The
 1802 Cryosphere, 13, 2615–2631, <https://doi.org/10.5194/tc-13-2615-2019>, 2019.
 1803 Toggweiler, J.R., Russell, J.L., Carson, S.R. Midlatitude westerlies, atmospheric CO₂, and
 1804 climate change during the ice ages. 2006. Paleoceanography and Paleoclimatology, 21,
 1805 <https://doi.org/10.1029/2005PA001154>.
 1806 Troch, M., Bertrand, S., Lange, C.B., Cardenas, P., Arz, H., Pantoja-Gutierrez, S., De Pol-Holz
 1807 R., Kilian, R. Glacial isostatic adjustment near the center of the former Patagonian Ice
 1808 Sheet (48S) during the last 16.5 kyr. Quaternary Science Reviews, 277.
 1809 <https://doi.org/10.1016/j.quascirev.2021.107346>
 1810 Yan, Q., Wei, T., Zhang, Z. Modeling the climate sensitivity of Patagonian glaciers and their
 1811 responses to climatic change during the global last glacial maximum. 2022. Quat. Sci.
 1812 Rev., 288. <https://doi.org/10.1016/j.quascirev.2022.107582>
 1813 Zech, J., Terrizzano, C.M., García Morabito, E., Veit, H., Zech, R., 2017. Timing and extent of
 1814 late Pleistocene glaciation in the arid Central Andes of Argentina and Chile (22°-41°S).
 1815 Geogr. Res. Lett. 43, 697–718. <https://doi.org/10.18172/cig.3235>.
 1816
 1817
 1818

Formatted: Default Paragraph Font, Font color: Text 1, Pattern: Clear

Moved (insertion) [5]

Formatted: Indent: Hanging: 0.5"

Deleted: ¶

Formatted: Font color: Text 1

Formatted: Indent: Hanging: 0.5", Line spacing: Multiple 1.1 li, No widow/orphan control, Border: Top: (No border), Bottom: (No border), Left: (No border), Right: (No border), Between : (No border)

Deleted: Quaternary sea

Formatted: Font color: Text 1

Formatted: Highlight

Formatted

Formatted: Default Paragraph Font, Font color: Text 1, , Pattern: Clear

Formatted

Formatted: Indent: Hanging: 0.5"

Formatted: Font: (Default) Times New Roman, 12 pt

Formatted: Default Paragraph Font, Font color: Text 1

Formatted: Font color: Text 1

Formatted: Indent: Hanging: 0.5"

Page 6: [1] Deleted Cuzzone, Joshua K (US 329C-Affiliate) 9/20/23 11:52:00 AM

Page 6: [2] Deleted Cuzzone, Joshua K (US 329C-Affiliate) 8/28/23 11:21:00 AM

Page 6: [3] Deleted Cuzzone, Joshua K (US 329C-Affiliate) 8/28/23 11:16:00 AM

Page 6: [4] Deleted Cuzzone, Joshua K (US 329C-Affiliate) 8/28/23 11:18:00 AM

Page 6: [5] Deleted Cuzzone, Joshua K (US 329C-Affiliate) 8/28/23 11:17:00 AM

Page 6: [6] Deleted Cuzzone, Joshua K (US 329C-Affiliate) 8/3/23 1:28:00 PM

Page 6: [7] Formatted Cuzzone, Joshua K (US 329C-Affiliate) 9/6/23 10:28:00 AM

Font: (Default) Times New Roman, 12 pt, Font color: Text 1

Page 6: [8] Formatted Cuzzone, Joshua K (US 329C-Affiliate) 9/6/23 10:28:00 AM

Font: (Default) Times New Roman, 12 pt, Font color: Text 1

Page 9: [9] Deleted Cuzzone, Joshua K (US 329C-Affiliate) 9/1/23 1:08:00 PM

Page 9: [10] Deleted Cuzzone, Joshua K (US 329C-Affiliate) 8/28/23 11:43:00 AM

Page 13: [11] Deleted Cuzzone, Joshua K (US 329C-Affiliate) 9/1/23 2:54:00 PM

Page 15: [12] Deleted Cuzzone, Joshua K (US 329C-Affiliate) 9/20/23 12:00:00 PM

Page 15: [13] Commented [CJK(3A6)] Cuzzone, Joshua K (US 329C-Affiliate) 8/4/23 11:03:00 AM

In fact Kohfield does extensive analysis of paleo proxies to suggest that changes in hydrologic cycle do not necessarily have to be linked to changes in SWW, and is only 1 possible explanation for these changes. “A chain of assumptions are needed to interpret paleodata as changes in the westerly wind position and intensity. Importantly, the modern relationships between Southern Hemisphere westerly winds and moisture must hold for past time periods, and over an increased latitudinal range at the LGM, compared with the present day. We also outline several caveats in interpreting changes in winds from SSTs and fronts, accentuating the complex relationship between SSTs, fronts, and westerly winds as well as the difficulty in resolving SST gradients and front positions based on limited SST data. These inherent assumptions, and the possibility for multiple interpretations of the observations, create uncertainty in conclusions regarding past changes in winds interpreted solely from data

“

And Then modelling from Sime et al., 2013: [Sime et al. \(2013\)](#) use this moisture reconstruction to assess impacts of LGM wind fields on moisture patterns from several AGCM and AOGCM simulations. Their results suggest that model simulations do a reasonable job of reproducing LGM moisture patterns without large shifts in glacial winds and provide one example of integrating model simulations with data compilations to understand ocean-atmosphere changes during the LGM.

Rojas 2013 find this as well PMIP2 models.

Therefore although hydrologic cycles change when looking at proxy data, uncertainty still exists regarding whether its due to SWW strength position or other explanations.

Jiang show Trace was more poleward at LGM, which disagrees with proxy data from the CLD indicating potential for Northward displacement of SWW (Moreno 1999, 2015)

|